Effect of environment on mechanical properties of 3D printed polylactide for biomedical applications

Amirpasha Moetazedian[1], Andrew Gleadall[1*], Xiaoxiao Han[1], Vadim V. Silberschmidt[1]

[1] *Wolfson School of Mechanical, Electrical and Manufacturing Engineering, Loughborough University, Loughborough, LE11 3TU, UK*

*****Corresponding author - Email: A.Gleadall@lboro.ac.uk

Journal of the Mechanical Behavior of Biomedical Materials

The final publication is available at https://doi.org/10.1016/j.jmbbm.2019.103510

Abstract

In this study, the importance of the testing environment for correct assessment of tensile strength of polylactide (PLA) is investigated. A novel design of tensile specimen was developed to test the anisotropic mechanical properties of additively manufactured specimens. The effects of three environmental factors were considered: physiological temperature (37˚C), hydration (specimens stored in solution for 48 hours) and in-aqua testing (specimens submerged in solution). For the first time, these factors were studied both individually and combined, and were evaluated against a control point (non-hydrated specimens tested in air at room temperature). The tensile strength and modulus of hydrated specimens tested submerged at 37˚C were reduced by 50.1% and 20.3%, respectively, versus the control. In contrast, testing the hydrated polymer in air at room temperature, which is commonly used to refer to wet strength in literature, only showed an 18.3% reduction in tensile strength with a negligible change in tensile modulus. To assess transferability of the results, additively manufactured specimens were also tested normal to the interface between 3D printed layers, and they demonstrated similar reductions in strengths and moduli. The results demonstrate the importance of using an appropriate methodology for tensile testing; otherwise, mechanical properties may be overestimated by two-fold.

Keywords: Biodegradable polymer, PLA, additive manufacturing, wet mechanical properties, submerged tensile testing, water absorption

1. Introduction

Polylactide (PLA) is an aliphatic polyester produced from renewable sources such as sugarcane [1], [2]. Thanks to its biodegradability and biocompatibility [2], [3], it is now one of the most studied biodegradable polymers [3]–[6]. PLA is used for various applications in the fields of aerospace, industry and medicine [7]–[9]; importantly, it is also 3D printable. With the current advances in technology, additive manufacturing (AM) revolutionised the manufacturing process and emerged as a viable tool to reduce production cost while accelerating product development [10]–[14]. In particular, manufacturing of customised medical devices such as

cranial fixations, screws and bone-plate fixation using biodegradable polymers has accelerated significantly [10]. One of the most common AM technologies for polymers is material extrusion (ME), which uses thermoplastic polymers (including PLA) to produce complex parts, which cannot be achieved with injection moulding [15]–[18]. In ME, a polymer filament is fed into a heated nozzle, liquefied and extruded onto a print bed, layer by layer, until the part is completed [19], [20]. The manufacturing strategy for ME parts can alter their mechanical properties. For instance, manufacturing-induced anisotropic properties are typically reported for parts 3D printed in an upright orientation as a result of incomplete fusion between layers [17], [21]–[23]. Therefore, a large number of studies have investigated various ways to improve the overall mechanical properties of additively manufactured parts [24]–[27].

Optimisation of mechanical properties of polymeric components for biomedical application is typically based on measuring them at ambient temperature. However, in biomedical applications, an implant is exposed to a different environment than that found in a laboratory, which can affect mechanical properties [28]. This is especially crucial for biodegradable polymers, where rapid water uptake could alter the structural stability via interaction with polymer chains [29]–[32]. An increased temperature additionally enhances this process.

Consequently, it is essential to consider and understand the effects of the testing environment that represents the *in vivo* conditions on properties of polymers, as they are sensitive to fluctuations in temperature and moisture [33]–[35]. The search of the Scopus database with terms “wet-state strength” or “wet strength” for synthetic biodegradable polymers for biomedical applications, demonstrated that many studies [28], [36], [45]–[50], [37]–[44] (shown in Table 1) have performed mechanical testing of dry or hydrated samples in laboratory conditions (i.e. at room temperature (RT)), as schematically shown in Figure 1a. Only few studies [51]–[54] measured the properties of natural polymers with the specimen fully submerged in solutions (i.e. water or phosphate buffer saline (PBS)), at RT or physiological temperature (PT, 37˚C), as shown schematically in Figure 1b and c, respectively. Furthermore, only one study was found which measured mechanical properties of PLA submerged in water at RT [55].

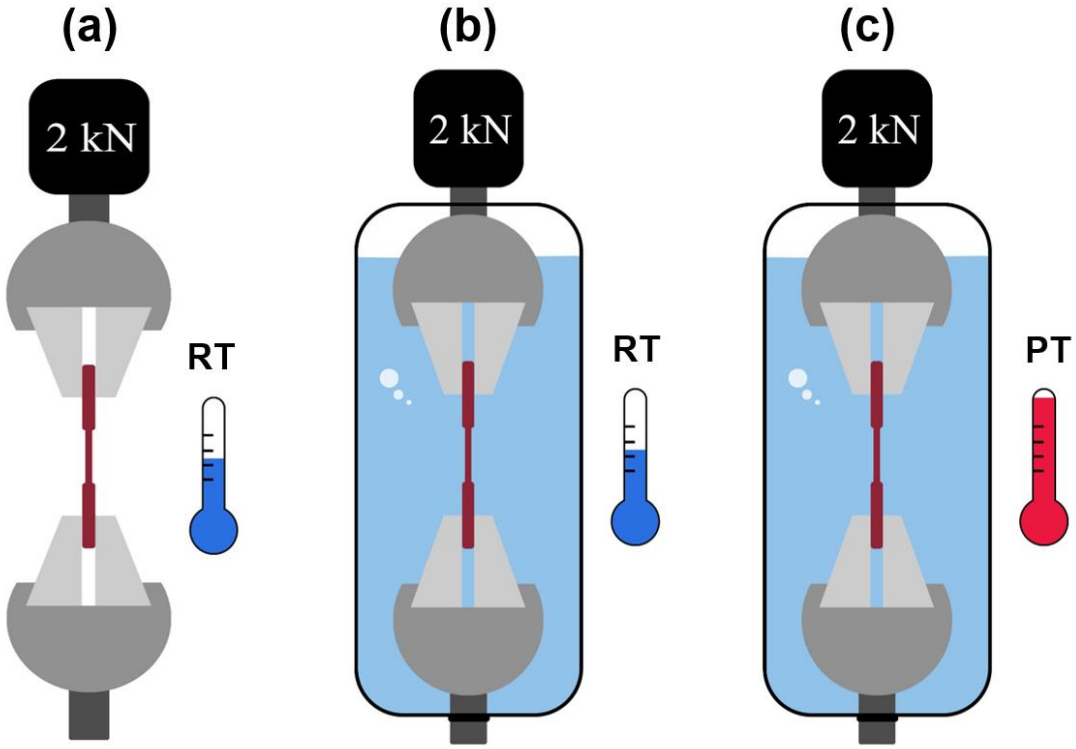

Figure 1 Schematic diagrams indicating different testing environment for mechanical testing: (a) in air at room temperature (RT), (b) submerged in water at RT and (c) submerged in water at physiological temperature (37˚C). Many studies measured the mechanical properties of dry or hydrated samples using set-up (a), while set-up (c) more adequately represents the actual environment of medical devices.

For instance, mechanical properties of dry and hydrated poly (lactic-co-glycolic acid) (PLGA) scaffolds were examined in study [28], and their compressive strength and elastic modulus at RT was found to decrease by approximately 20% and 35% respectively upon hydration in PBS compared to those tested dry. In the same study, the glass transition temperature (T_g) of the hydrated scaffold was lower than that of the dry samples, and the plasticising effect of water in PBS was believed to be responsible. A number of other studies [56]–[59] also reported an adverse effect of water, resulted in a considerable change in visco-elasticity, toughness and tensile strength of polymers [28], [33], [58]. Some studies [28], [35], [47], [59], [60] also examined the effect of different temperatures on mechanical properties of dry or hydrated polymers; it was shown to be similar to the effect of water. Most studies summarised in Table 1 highlighted the strong influence of both water absorption and temperature on the mechanical performance of various polymers. However, these studies conducted the tensile testing predominately at laboratory conditions or increased temperatures without considering the submerged testing environment. All studies with submerged mechanical testing considered natural polymers such as silk and collagen [52], [54], [61], [62], meanwhile there is only one study [55] which considered submerged testing of PLLA at RT. It is therefore critical to determine the effect of environmental factors (water and higher temperature) on mechanical properties of polymers. To the best of the authors' knowledge, no direct comparison was implemented between dry and hydrated samples, tested at RT and PT in submerged and unsubmerged conditions for biodegradable polymers. Thereby, this study aims to determine the influence of three different aspects of testing conditions on mechanical properties:

- dry vs. hydrated polymer
- room temperature vs. physiological temperature testing conditions
- unsubmerged vs. submerged testing conditions

Table 1 Different testing environments and conditions used in previous studies to measure mechanical properties of synthetic polymers. Most studies only compared dry to hydrated samples for mechanical tests at RT. No studies measured the mechanical properties of synthetic polymers submerged in water at 37˚C or compared the combined effect of hydration, submerged and increased temperature. PLGA- poly (lactic-co-glycolic acid); ABS- acrylonitrile butadiene styrene; PA- polyamide; PVC- polyvinyl chloride.

Type of polymer		Material	Testing conditions			Measured properties	Study
			Dry vs. hydrated	Submerged vs. un-submerged	RT vs. PT		
Synthetic polymers	PLA	PLA	✓	✗	✗	Tensile strength, tensile modulus and elongation-at-break	[36]
		PLA	✓	✗	✗	Tensile strength	[37]
		PLLA	✓	✗	✗	Tensile strength and tensile modulus	[38]
		PLLA	✗	✗	✗	Compressive strength and compressive modulus	[51]
		PLA nanofibre	✓	✗	✗	Tensile strength, tensile modulus and elongation-at-break	[39]
		PLA + Titanium	✓	✗	✗	Adhesion strength	[40]
		PL/DLA-Dextran	✓	✗	✗	Tensile strength, tensile modulus and elongation-at-break	[41]
		PLA-PEG-PLA	✓	✗	✗	Compressive modulus	[42]
		PLA-PEG	✗	✗	✗	Tensile modulus	[52]
		PLA and PLA + chitosan	✓	✗	✗	Tensile strength, tensile modulus and elongation-at-break	[43]
		PLA	✗	✗	✓	Tensile strength and tensile modulus	[35]
		PLA	✗	✗	✓	Tensile strength, tensile modulus and elongation-at-break	[59]

		PLLA	✓	✓	✗	Tensile strength and tensile modulus	[55]
		PLA + phosphate glass fibres	✗	✗	✗	Flexural and compressive strengths	[48]
		PLA + collagen	✓	✗	✗	Tensile strength and tensile modulus	[50]
		PLA + alginate	✗	✗	✗	Tensile strength, tensile modulus and elongation-at-break	[49]
	PLGA	PLGA	✓	✗	✓	Tensile strength and tensile modulus	[44]
		PLGA	✓	✗	✓	Compressive strength and compressive modulus	[28]
		PLGA + hydroxyapatite	✓	✗	✗	Compressive strength and compressive modulus	[45]
		PLGA and PLGA + collagen	✓	✗	✗	Tensile strength	[46]
	ABS	ABS and ABS + copper or iron	✗	✗	✗	Tensile strength and tensile modulus	[63]
		ABS	✓	✗	✓	Tensile strength, tensile modulus and elongation-at-break	[47]
	PA	PA and PA + TiO_2 or clay	✗	✗	✗	Tensile strength, tensile modulus and elongation-at-break	[64]
	PVC	PVC + plasticiser	✗	✗	✓	Tensile strength and tensile modulus	[60]

2. Materials and method

2.1. Materials and 3D printing strategy

For this study, novel filament-scale micro-tensile testing specimens were produced using a natural polylactide filament with a diameter of 1.75 mm (3DXTECH® branded NatureWorks® polylactide 4043D, Sigma Aldrich). A RepRap x400 3D printing system was used to deposit four single filaments in a square and then repeated for 225 layers using the printing conditions given in Table 2. A four-sided hollow box with dimensions of 45 mm (height) x 45 mm (width) was printed as shown in the Figure 2a.

Table 2 Printing conditions used in RepRap x400 system

Description	Value
Nozzle diameter	0.4 mm
Nozzle temperature	210°C
Print-bed temperature	60°C
Printing speed	1000 $mm.min^{-1}$
Layer height	0.2 mm

Custom G-Code (a series of commands code to control the actions of a 3D printer) was used to produce novel dogbane tensile-testing specimens, with filaments width varying from 0.75 mm (shoulder region) to 0.50 mm (gauge region). The specimen geometry was adapted from the test specimen geometry described in the ASTM D1708-18 standard. As is well known, AM can produce a wide range of properties depending on the printing design and process; in this study, the effect of manufacturing process and design was also considered. Consequently, the two printing designs were chosen. First, “filament direction” specimens (Figure 2b) to assess the bulk properties by mechanically testing the filaments orientated in direction of the uniaxial load; these specimens were used for the majority of this study. The results are compared to bulk polymer specimens in other studies in Section 3.4 to ensure the specimens effectively represent bulk polymer. Second, “Z-direction” specimens to characterise the manufacturing-induced anisotropy between layers and consider interface strength, as shown by Figure 2c. Throughout this paper, the acronyms of F and Z are used to refer to respective printing directions. The custom G-Code provided a number of advantages compared with the conventional 3D printing slicing software, including precise control over:

- printing speed, which was kept constant during the extrusion since there was no change in the printing direction within specimens.
- extrusion rate, by extrusion of the same volume at all regions (partially enabled by the constant printing speed).
- cooling time, since all the extruded filaments were directly deposited on top of one another, the time between layerwise deposition at every point on every layer was constant, reducing the thermal variation.

The corners of the printed box were cut using disposable blades and a customised rig. The walls were then cut into 5 mm-wide specimens using disposable blades and a hydraulic press (to ensure controlled pressure during cutting). The dimensions of all specimens were 45 mm (height) x 5 mm (width) with a thickness in the gauge region of 0.5 mm.

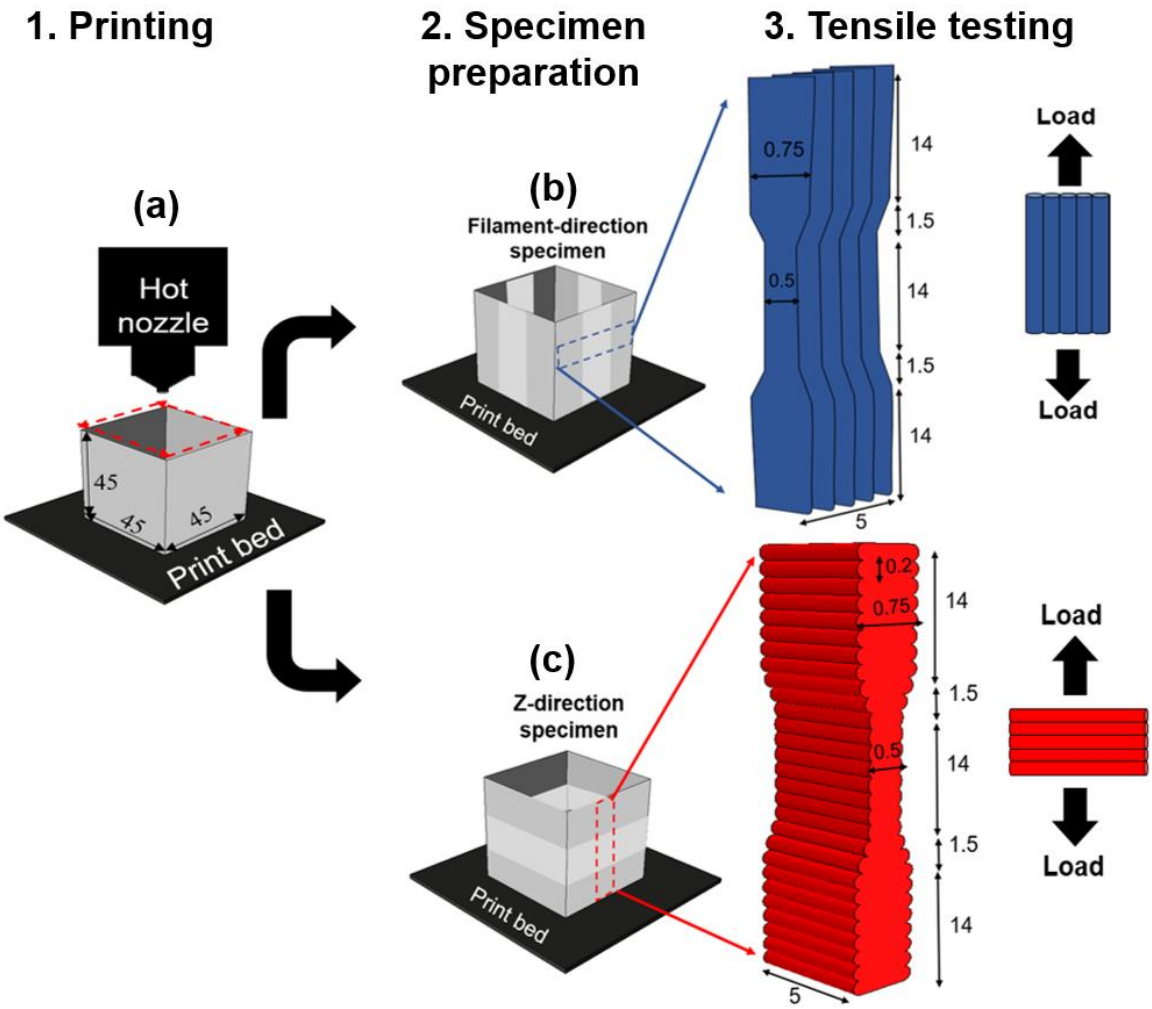

Figure 2 (a) Novel printing toolpath depositing a stack of single extruded filaments to produce the hollow box. (b) F specimens for testing along the filament direction. (c) Z specimens for tests normal to interface between filaments. The dimensions are in mm. A transitionary region (from shoulder to gauge) of 1.5 mm was used to ensure that specimens fractured in the gauge area.

2.2. Characterisation

2.2.1. Testing environments and conditioning of specimens

3D printed tensile specimens (n=5) were used either as manufactured (dry) or stored in 30 ml of deionised water for a period of 48 hours at PT (hydrated). Tensile tests were implemented in air or with specimens submerged in water as shown in Table 3 and Figure 3. Five different testing conditions were used:

- Dry specimens were tested in air at RT (S_{Ref}), which were considered as control group.
- The effect of water absorption was investigated by testing hydrated specimens in air at RT (S_H).
- Dry specimens were also tested in air at 37˚C to only assess the effect of physiological temperature (S_P).
- For submerged tensile testing, dry (i.e. not hydrated) specimens were tested at RT (S_S) to only consider the effect of water-submersion during experiments.

- For the final group, hydrated specimens were tested at PT submerged in water (S_{PHS}) to investigate the combined effect of all three conditions.

Table 3 Different testing environments used in this study.

Specimen name	Testing environment	Testing temperature	Specimen state	Condition varied compared to control
S_{Ref}	Air	RT (20˚C)	Dry	-
S_H		RT (20˚C)	Hydrated	Hydration
S_P		PT (37˚C)	Dry	Physiological temperature
S_S	Submerged	RT (20˚C)	Dry	Submerged testing
S_{PHS}		PT (37˚C)	Hydrated	All three factors above

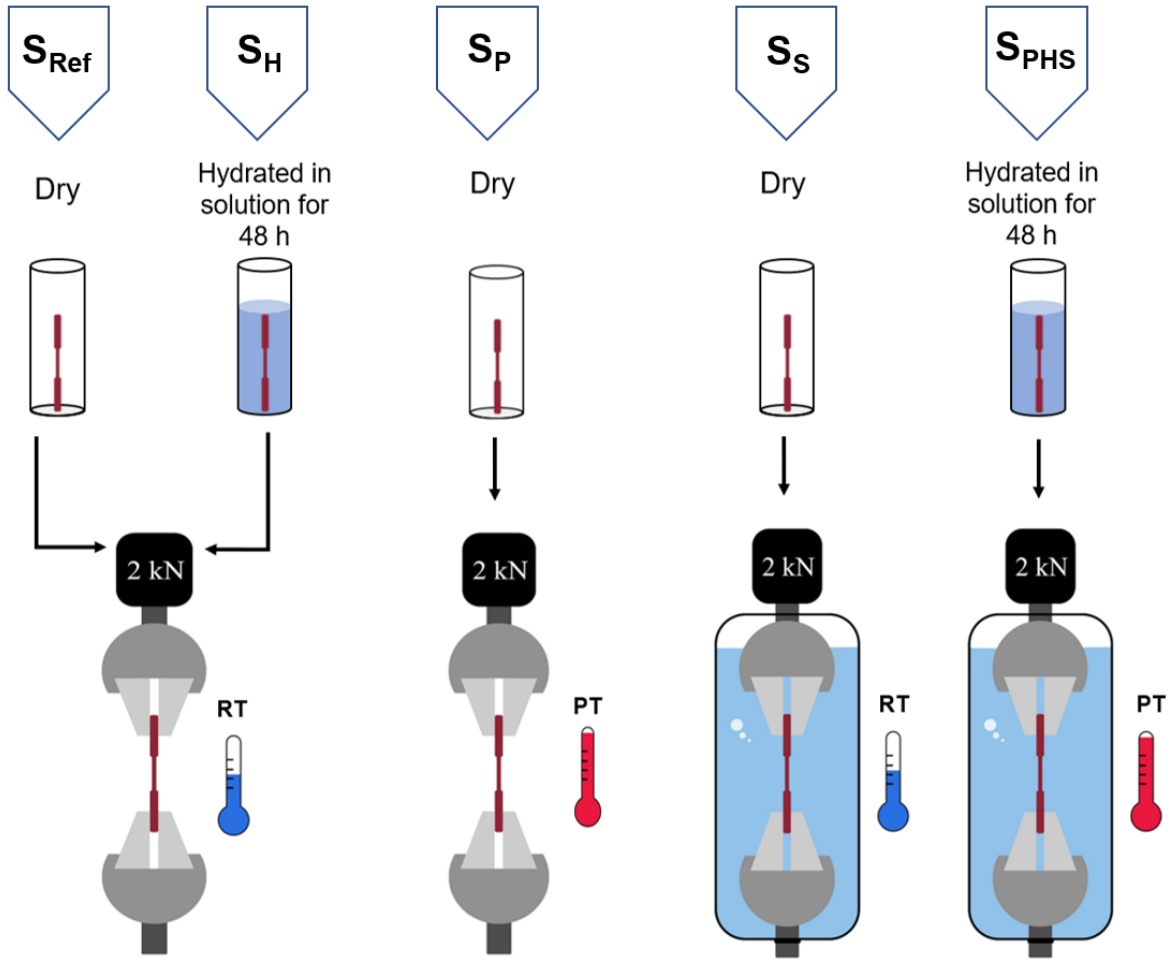

Figure 3 Different testing environments used in this study: dry specimens tested in air at RT (S_{Ref}); specimens hydrated initially for 48 hours and then tested in air at RT (S_H); dry specimen tested in air at PT (S_P); dry specimens tested submerged at RT (S_S) and hydrated specimens tested submerged at PT (S_{PHS}).

2.2.2. Tensile testing

A universal mechanical testing machine (Instron 5944, USA) was equipped with a BioPlus Bath system including temperature-controlled bath (Instron BioPlus, Instron, USA) and a 2 kN load cell, employed at displacement rate of 0.5 mm.min^{-1} (strain rate of 4.10^{-4} s^{-1}). The tensile tests were performed under the environmental conditions described in Table 3. For submerged tensile testing at PT, the specimens were initially left in the water for 30 min prior to the start of the test to reach the uniform temperature. A Zeiss Primotech microscope was used to assess a pre-fracture surface area for strength calculation. For Z specimens, the fracture always occurred at the weakest section (i.e. the interface bond between filaments). As a result, the mean value for measurements of at least 10 bond widths for each Z specimen was used to calculate the cross-sectional area. To calculate the cross-sectional area of F specimens, the following method was utilised:

1. Cross-sectional areas of at least ten individual filaments were measured to obtain the mean value;
2. This mean value was then multiplied with the number of filaments in the specimen (25).

The tensile modulus for each specimen was obtained using a linear elastic region obtained from stress-strain curves. To distinguish between Z and F specimens tested at different conditions, the superscript Z was added to the respective parameters for the Z specimens tested at different conditions (e.g. S^Z_{Ref}, S^Z_S etc).

2.2.3. Thermal analysis

To characterise thermal properties, S_{Ref} (dry) and S_H (hydrated) specimens (n=2) were analysed using differential scanning calorimetry (DSC) with a TA Q2000 instrument (TA instruments, USA). Specimens with a weight of 5-10 mg were loaded onto the aluminium pans and heated to temperatures ranging from 30 to 200°C at a ramping rate of 10°C.min^{-1} in a nitrogen atmosphere (flow rate of 50 ml.min^{-1}). The crystallinity Xc (%) of the PLA specimen was calculated using Equation 1.

$$Xc = \frac{\Delta H_m - \Delta H_{cc}}{\Delta H_m^0} \times 100\% \quad (1)$$

where ΔH_m is the melting enthalpy (J.g^{-1}), ΔH_{cc} is the enthalpy of cold crystallisation (J.g^{-1}) and ΔH^0_m is the enthalpy of fusion for 100% crystalline PLA which is 93.1 J.g^{-1} [32].

2.2.4. Water-absorption analysis

The initial weight (W_0) of dry specimens (n=3) straight after the cutting process was measured using an analytical balance with precision of ± 0.0001 g (Ohaus Adventurer, Switzerland). Subsequently, they were stored in 30 ml water at RT and PT. At different time intervals; 0.5 h, 12 h, 24 h and 48 h, each specimen was taken out and the excess water was removed with a cloth. Then, the wet weight (W_1) was measured. The mean water absorption ΔW was then calculated using Equation 2 [65].

$$\Delta W = \frac{W_1 - W_0}{W_0} \times 100\% \quad (2)$$

2.2.5. Optical microscopy

After tensile testing, the fracture surface for each group was examined using an optical Zeiss Primotech microscope at magnification 5x.

2.2.6. 3D surface analysis

Alicona G4 InfiniteFocus (Bruker, Germany) was employed to perform high-resolution 3D scans of the fracture surface for all groups of the specimens. In this technique, topographical information is provided by combination of vertical scanning and focusing of the optical system at different depths (focus-variation technique). Scans were acquired at a magnification of 10x for the entire surface and at higher magnification of 20x for left, middle and right segments of the total area to extract more information about the surface roughness. The scans were post-processed using Mountains Premium 7.4 software (Digital surf, France) to create colour-height mapping of the surface.

2.2.7. Statistical analysis

The data obtained for water absorption and mechanical properties were expressed as means ± standard deviation (SD). The appropriate statistical analyses with Analysis ToolPak in Excel 2016 such as one-way analysis of variance (ANOVA) and subsequent t-test at significant levels of $p<0.05$, $p<0.01$ and $p<0.001$ were used.

3. Results and discussion

In this section, first, the process of water absorption over 48 hours is characterised to check saturation. Subsequently, the mechancial properties of F specimens (defined in Figure 2), which are used in this study to represent bulk polymer, are investigated for the five different testing conditions given in Table 3 and Figure 3. Finally, Z specimens (defined in Figure 2) are tested to determine whether the trends identified for bulk polymer are affected by manufacturing conditions.

3.1. Water-absorption studies

In the first step, the evolution of water absorption of PLA was examined. Its magnitude as a function of immersion time (Figure 4) at RT and PT was plotted to compare the effect of temperature on the process. After 30 min, water absorption reached 0.561% and remained constant over 48 hours as there was no significant difference ($p = 0.781$) between 30 min and 48 hours of hydration similar to previous studies [65], [66]. Increasing the water temperature to 37°C, increased its absorption significantly ($p = 0.017$) to 0.741%, indicating a strong influence of temperature on water uptake [67]. Once again, no statistical difference was found for hydration between 30 min and 48 hours hydration ($p = 0.700$).

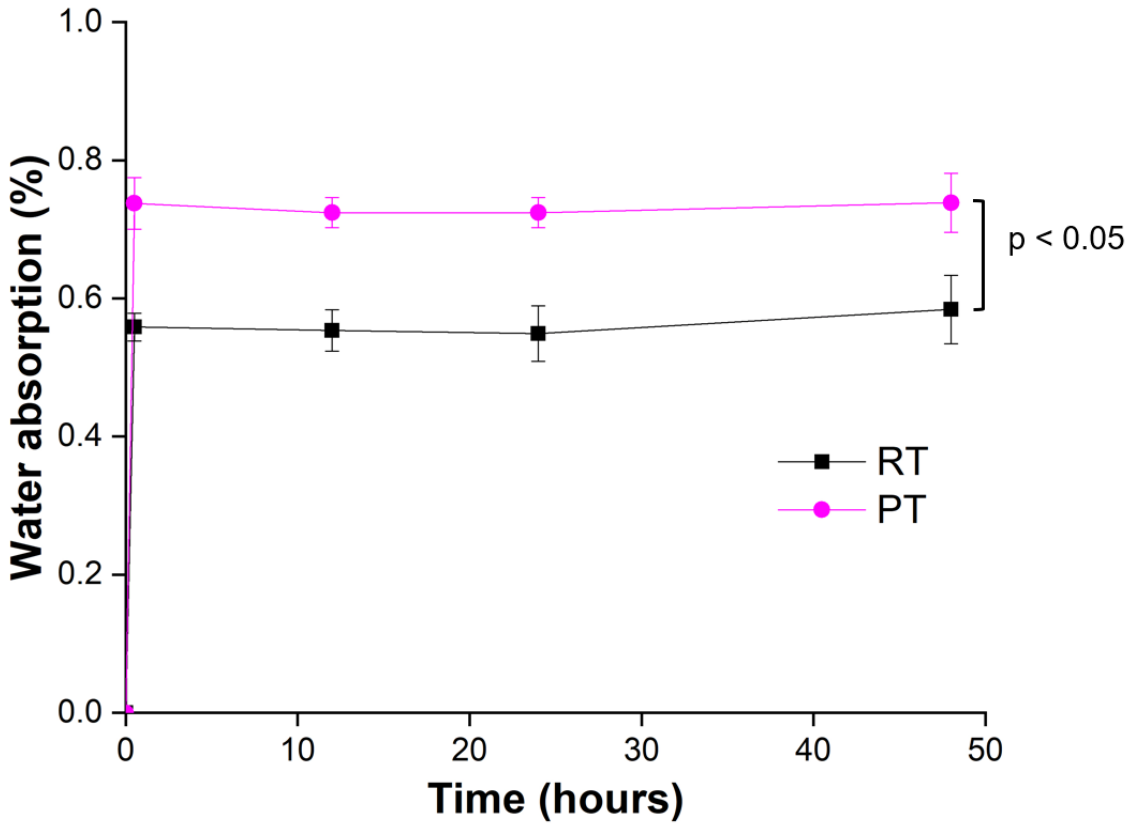

Figure 4 Evolution of water absorption with time for specimens stored at two temperatures. The water absorption reached 0.561% at RT, whereas storing the polymer at PT allowed more water to be absorbed ($p<0.05$). In both cases, the levels of absorption remained constant over 48 hours.

The submerged tensile testing for different hydration periods in the water at both RT and PT is shown in Figure 5. There is no data point for 0 hours since all specimens in this study were submerged for 30 min before the tests to ensure the uniform temperature. The mean ultimate tensile strength (UTS) values did not decrease significantly ($p = 0.188$) from 30 min to 48 hours of hydration. This results showed the immediate plasticising effect of water molecules even after 30 min (previously shown for hydrated samples tested at RT [28]) and after that the effect of water remained relatively constant since no further water absorption happened. On the other hand, from the Figure 5, the sensitivity of PLA to testing temperature is evident: increasing the temperature from RT to PT significantly weakened the polymer by 23.4% ($p = 1.38 \times 10^{-5}$). This highlights the dependency of mechanical strength of polymers on the in-service temperature [59], [60], since at a higher temperature more water molecules could penetrate the material due to the increase in the segmental mobility [32]. The relationship between mechanical properties and temperature is analysed in the next section of this study.

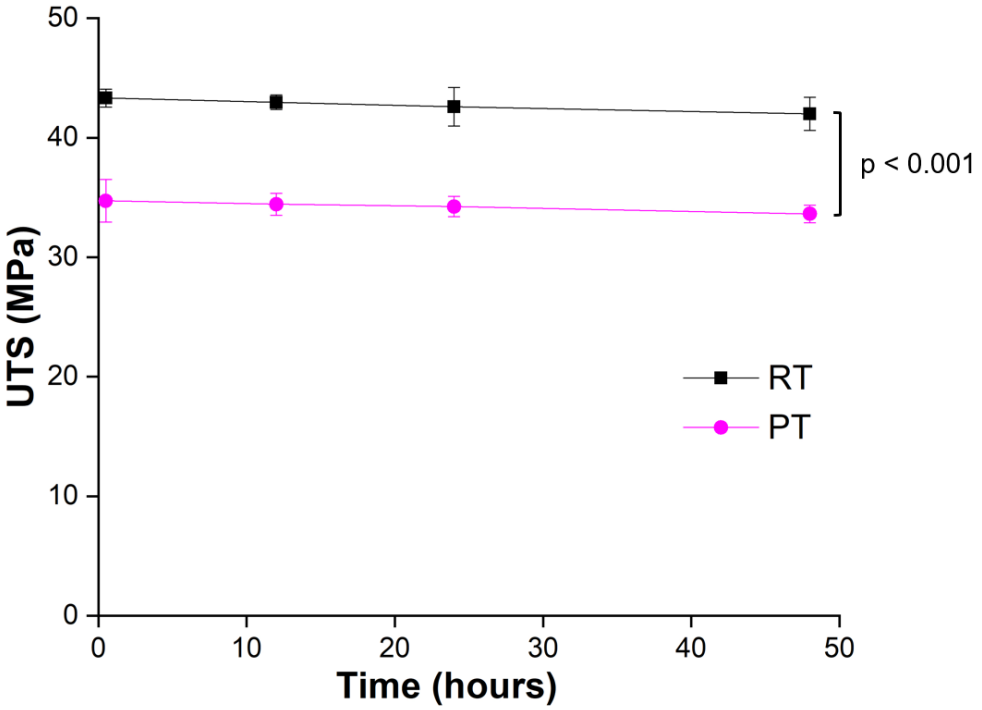

Figure 5 Evolution of the mean UTS for submerged testing with hydration time. There was no significant difference in the mean UTS values between 30 min and 48 hours. Testing at PT as opposed to RT significantly ($p<0.001$) reduced the strength at all time periods.

3.2. Effect of testing environment on mechanical properties

The stress-strain curves for all F specimens tested at different environments are presented in Figure 6. Mean values of UTS, tensile modulus, strain at maximum force and break were extracted from the curves and presented in Figure 7. The stress-strain curves showed a well-defined yield stress for all the specimens. The reference specimen (S_{Ref}) had the highest levels of tensile strength and modulus. Both of these properties reduced by testing under conditions of (from least to most significant) hydration (S_H), increased temperature (S_P) and submerged (S_S). The S_{PHS} specimens (tested with all three of the investigated conditions combined, which is closer to conditions in the human body) demonstrated the lowest strength (50.1% reduction) and modulus (20.3% reduction). The testing was also conducted in PBS and showed little difference compared to that of water (3.49% and 4.96% in strength and modulus respectively), suggesting that the water present in the solution plays the major role in changing the properties of the polymer. The next four subsections discuss the results of each testing condition individually.

3.2.1. Effect of temperature

The results in Figure 6 and Figure 7 indicated the strong influence of temperature on mechanical properties of PLA. The higher temperature significantly reduced the UTS ($p = 2.1 \times 10^{-10}$) of dry specimens (S_P versus S_{Ref}) by approximately 23%, which was within the range observed in previous studies [28], [35], [59]. Thermal characterisation of 3D printed PLA specimens using DSC revealed that the T_g of S_{Ref} was 60.7˚C (Figure 8). Tensile testing at RT would mean that the gap between the testing temperature and T_g of the printed part was approximately 35˚C, and polymer-chain mobility was more likely to be limited than for PT [64]. Increasing the environment's temperature to 37˚C reduced this gap causing higher chain mobility by allowing more molecular segment motions [33], [59], [64]. This could explain the increase in the strain at break and reduction in the strength.

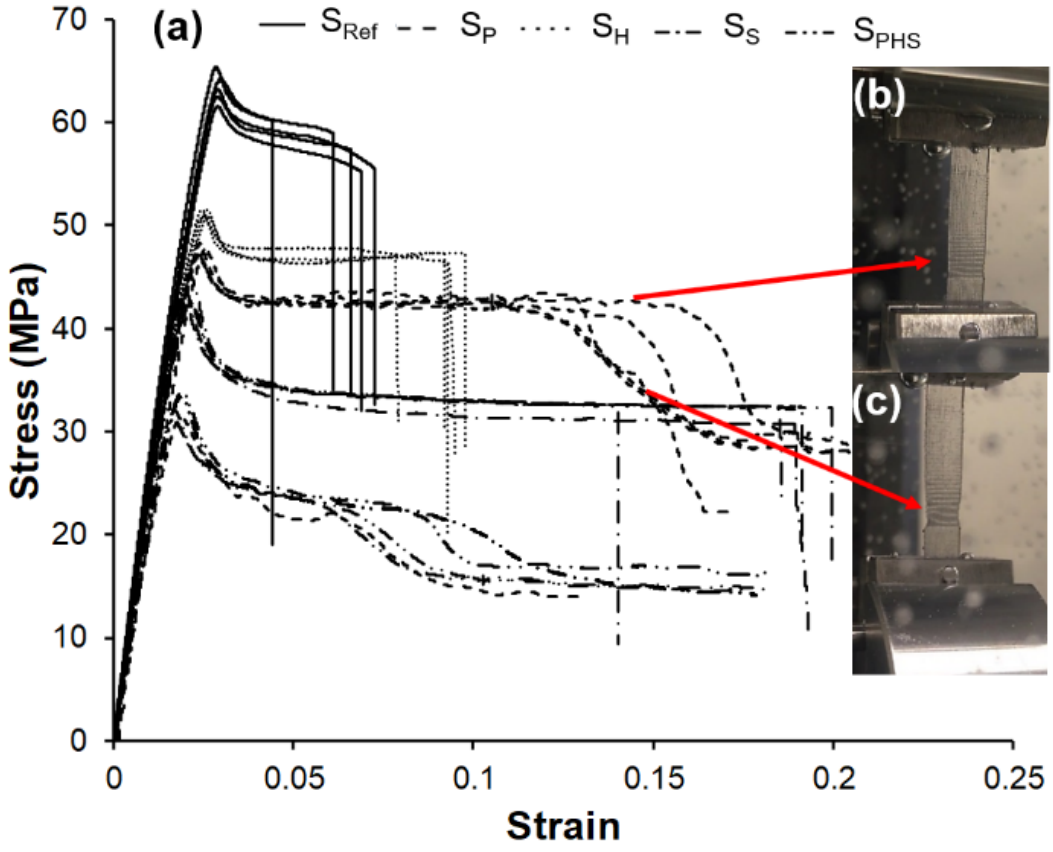

Figure 6 (a) Stress-strain curves of specimens tested at different testing conditions. A decreasing trend in the strength values in the order $S_{Ref}>S_H>S_P>S_S>S_{PHS}$ was observed. Specimens tested dry or submerged at PT showed the onset of necking (b) and continued to deform (c) without failing up to 40 % strain. Specimens tested in air at RT failed after 6.41% strain.

The higher temperature also changed the mechanical performance of PLA by preventing the failure of the polymer, possibly by re-orientation of chains under the uniaxial load, allowing greater extension of the material before failure [59]. This behaviour was reported in a previous study, in which PLA was tested at a temperature closer to its T_g [68]. The onset of extensive necking at 37˚C might be explained by low crystallinity of 3D printed specimens (X_c = 3.02% in Figure 8). The change in temperature could have adversely affected the amorphous regions and enabled the polymer chains to move freely [59], [69]. Another distinct difference for specimens tested at PT was the onset of necking (Figure 6b and c) which continued to final deformation up to 40% possibly due to cold-drawing of polymer chains into the local necking region. There was a 10.3% reduction in the tensile modulus under increased temperature ($p = 1.48 \times 10^{-5}$), similar to values previously reported [28], [35], [59]. The structure of PLA is

composed of stiff crystalline and entangled amorphous regions [35], [70], and the resistance of both phases to loading determines the modulus within the elastic region [35], [70]. At PT, movement of the amorphous phase could be activated, although the crystallite phase was more likely to stay unchanged thanks to its higher thermal stability [35], [70]. Since the polymer in this study was mostly amorphous, the reduction in resistance of the amorphous phase caused by the increasing temperature was sufficient to lower the modulus significantly as shown in Figure 7b [36], [63].

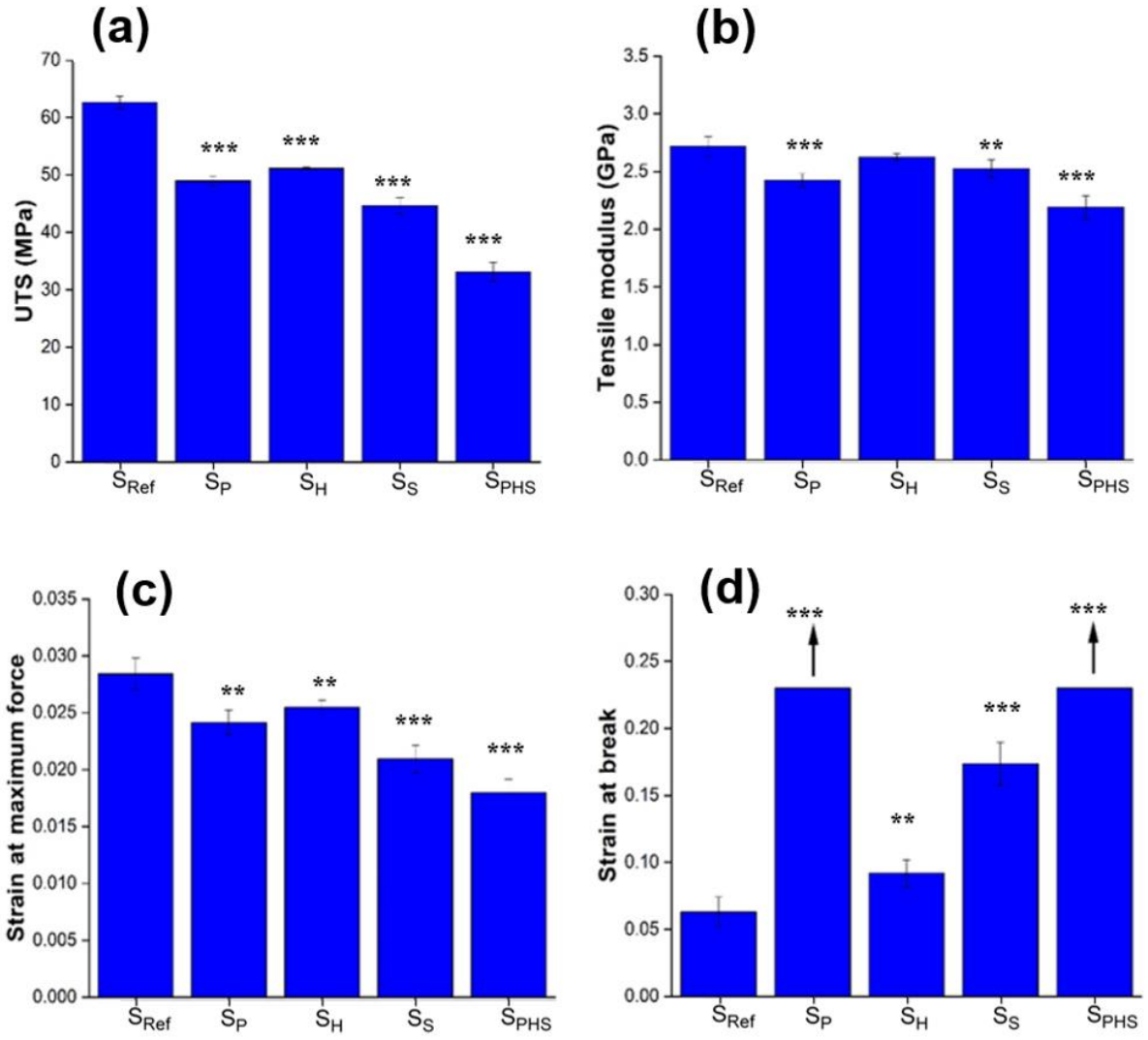

Figure 7 Mean UTS (a), tensile modulus (b), strain at maximum force (c) and strain at break (d) for different testing environments. Both temperature and in aqua environment significantly affected mechanical properties. The smallest effect was observed for S_H, whilst the highest one was when specimens were tested submerged at PT e.g. S_{PHS}. The arrows for S_P and S_{PHS} indicate continued deformation of material without failure to 40% strain (* $p<0.05$, ** $p< 0.01$ and *** $p<0.001$ compared with S_{Ref}).

3.2.2. Effect of hydration

Hydration of specimens prior tensile testing plasticised the polymer and reduced UTS ($p = 6.1 \times 10^{-9}$), strain at maximum force ($p = 6.10 \times 10^{-3}$) and increased the strain at break significantly ($p = 2.52 \times 10^{-3}$) compared with the S_{Ref}. Hydrated specimens showed lower levels of T_g and crystallinity compared to those of S_{Ref}, which further indicating the importance of considering the presence of water and its plasticising effect [28], [33], [41]. The reduction in the tensile modulus, on the other hand, was negligible ($p = 2.57 \times 10^{-1}$). Such behaviour was previously

observed for poly (hydroxyl ester ether), where water absorption of 0.511% reduced the UTS by 17.1%, while, the modulus was only lowered by 5.13% [33]. This also highlights that modulus is more temperature-sensitive and, therefore, for applications of polymers in humid environment at a higher temperature, the measurement of hydrated samples at RT could be misleading. Most studies (20 out of 24 from Table 1) obtained wet mechanical properties of hydrated specimen in this way (i.e. tested in air at RT). The results of our study indicate that, such conditions have less effect than those considered in Figure 7.

3.2.3. Effect of submerged testing

For the specimens tested submerged (to replicate the presence of fluid around the polymer in physiological conditions), the adverse effect of water during the test became more prominent even on tensile modulus (Table 4). Depending on the content and type of interactions, water molecules can exist in different states, including free water [32], [71], responsible for the plasticising effect [32], [71]. From the obtained results, the free water surrounding polymer could form clusters and disrupt the existing intermolecular interactions during the test [32], [71]. These factors could contribute to the plasticisation of polymer and thus, reduced its mechanical properties to a greater extent compared with those of the S_H condition. The combination of environmental factors (e.g. S_{PHS}) which is closer to *in vivo* conditions showed the largest influence by producing a synergistic effect and reducing the UTS by 50.1%, the modulus by 20.3% and strain at maximum force by 37.2%. The obtained results undoubtedly indicated the importance of testing environment for the mechanical properties of biodegradable polymers. Even though PLA is hydrophobic, the submerged tests showed a considerable change in the key mechanical properties as compared with the un-submerged environment.

Table 4 Summary of statistical analysis for different testing conditions and corresponding p values to indicate significance.

Property	Statistical analysis of data	
	Testing conditions	**p-value for testing conditions against reference S_{Ref}**
UTS	S_P	p<0.001 (p= 2.14E-10)
	S_H	p<0.001 (p=6.06E-09)
	S_S	p<0.001 (p=3.80E-06)
	S_{PHS}	p<0.001 (p=4.03E-09)
Tensile modulus	S_P	p< 0.001 (p=3.49E-04)
	S_H	No significance (p=1.23E-01)
	S_S	p<0.05 (p=1.88E-02)
	S_{PHS}	p<0.001 (p=1.48E-05)
Strain @ max. force	S_P	p<0.01 (p=1.24E-03)
	S_H	p<0.01 (p=6.10E-03)
	S_S	p<0.001 (p=5.10E-04)
	S_{PHS}	p<0.001 (p=1.22E-06)
Strain @ break	S_P	p<0.001 (p=1.74E-07)
	S_H	p<0.01 (p=2.52E-03)
	S_S	p<0.001 (p=1.00E-03)
	S_{PHS}	p<0.001(p=1.74E-07)

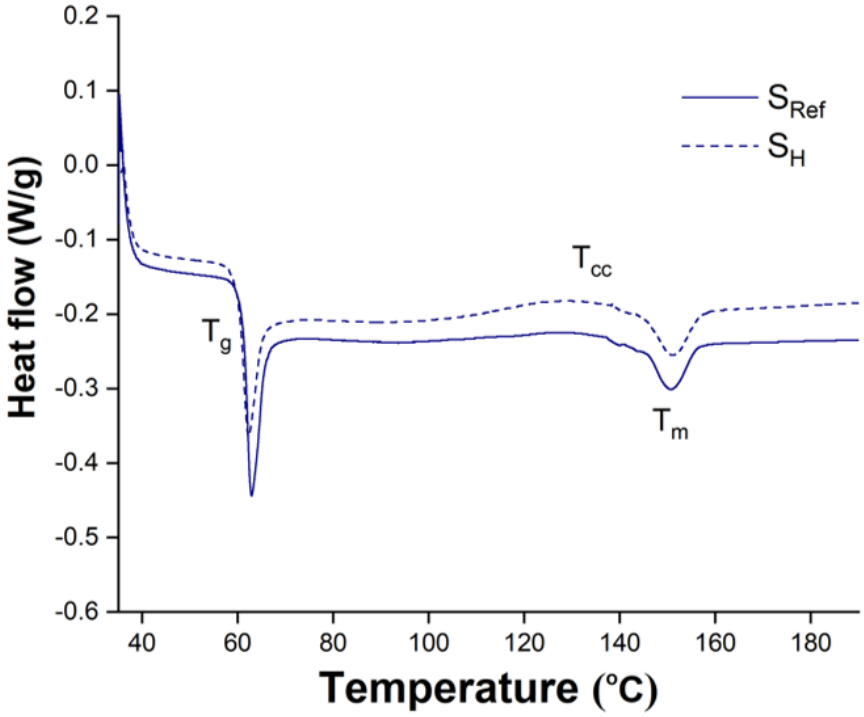

Testing condition	T_g (°C)	ΔH_m (J.g^{-1})	ΔH_{cc} (J.g^{-1})	X_c (%)
S_{Ref}	60.7 ± 0.02	3.48 ± 0.101	0.671 ± 0.04	3.02 ± 0.164
S_H	58.3 ± 0.24	3.17 ± 0.164	1.031 ± 0.24	2.30 ± 0.082

Figure 8 DSC curves obtained for S_{Ref} and S_H with the corresponding data indicating the values of T_g and calculated crystallinity (X_c). Hydration of specimens lowered both T_g and X_C.

3.2.4. Fractography analysis

Fractography analysis allows better understanding of fracture mechanisms. Optical micrographs for S_{Ref}, S_H and S_S showed the fracture features at the edges of the filaments as indicated in Figure 9. The filament width for the S_S specimen (indicated by dashed arrow) was on average 44 µm shorter than S_{Ref} due to the considerable plastic deformation (necking) prior to failure (Figure 9). The extent of plastic deformation was evident at higher magnification (right-column images) by the apparent necking of the filaments (shown by solid arrows in Figure 9). Necking of filaments was more pronounced for the submerged tests due to the increase in the material's ductility. The characterisation of surface roughness of these specimens using a focus-variation scheme (Figure 10) showed an increasing trend in the order $S_{Ref} < S_H < S_S$, which further confirmed the plasticising effect of water molecules and the growing ductility of the material.

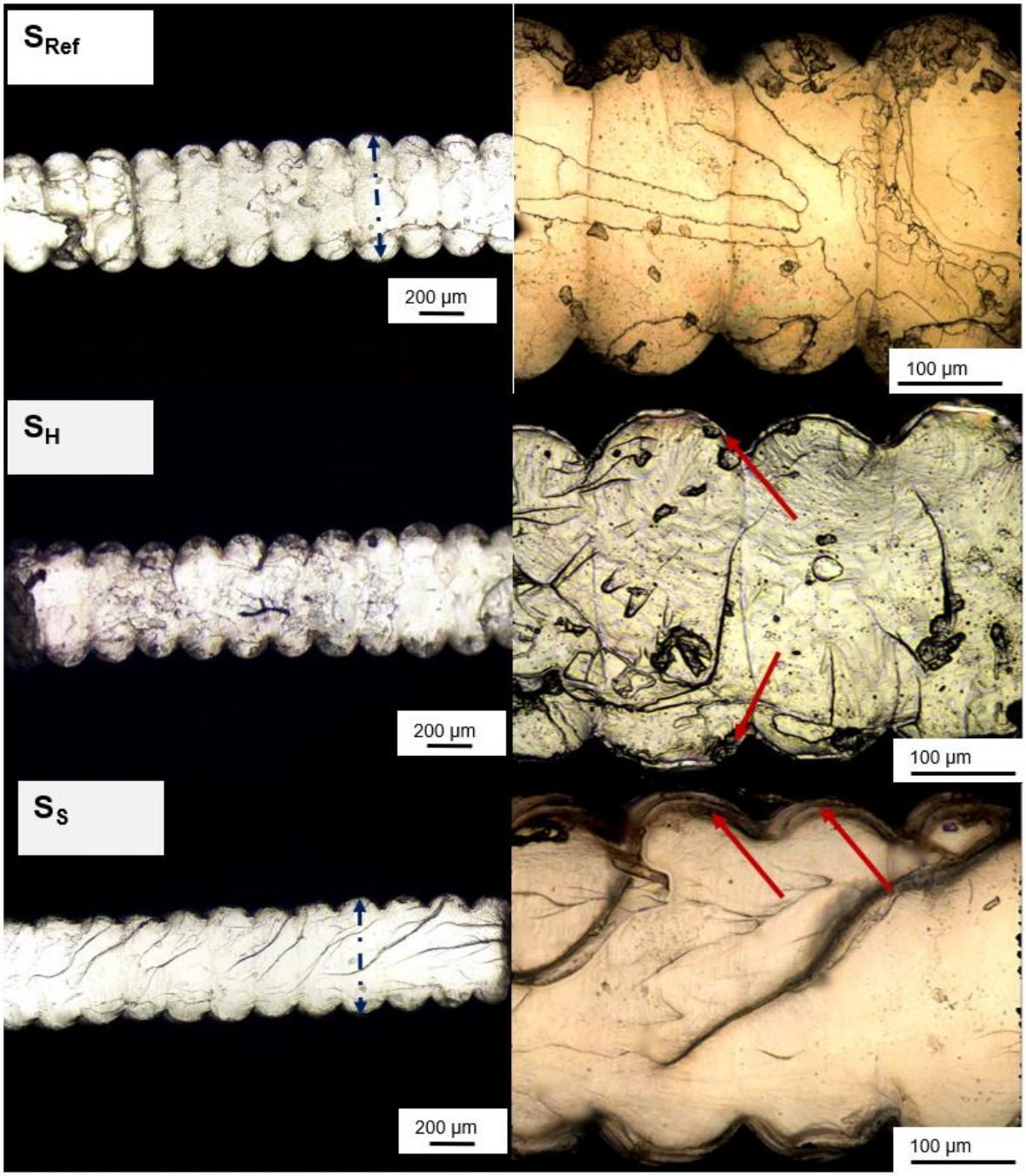

Figure 9 Optical microscopy images of fracture surfaces of F specimens. The S_{Ref} demonstrated the presence of multiple horizontal patterns at the interface bonds, whereas S_S showed vein-like patterns, starting mainly from the edges and moving towards the centre. S_S filaments (dashed arrow) were on average 44 µm shorter than S_{Ref} due to higher plastic deformation. At higher magnification (right-column images), the necking of the filament could be observed (as shown by the solid arrows).

The extracted surface profile for the left-column images in Figure 10 exhibited the shear lips characteristic for ductile fracture [72]. From the surface profiles (right-column images in Figure 10), it is apparent that the height of shear lips increased for tests performed on submerged specimens due to greater plasticity. The vein-like patterns for S_S were signs of internal necking (left-column images in Figure 10), which continued throughout the whole thickness. This could also explain the reason that the material did not fail when tested at PT.

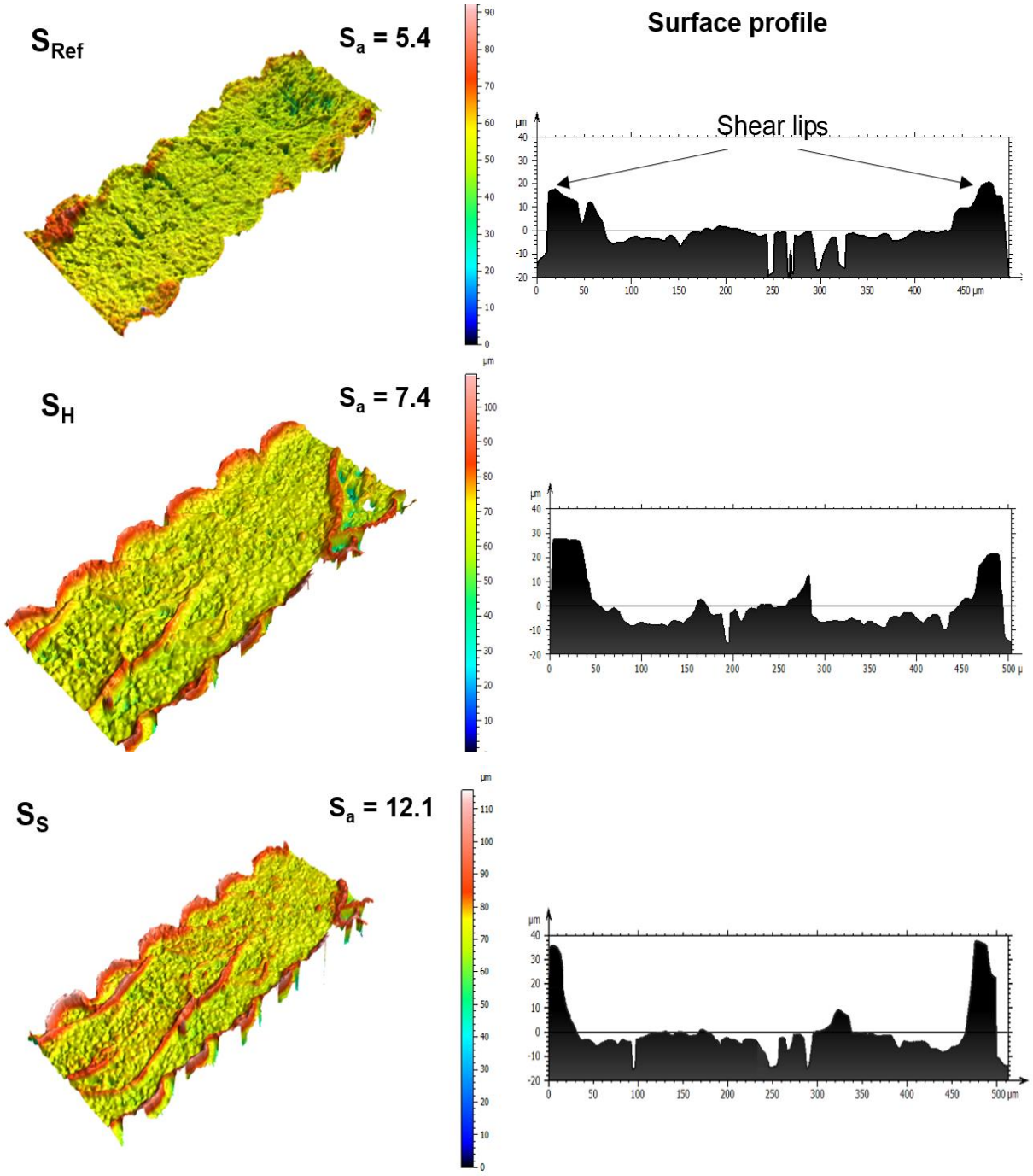

Figure 10 3D colour-height mapping images of fracture surfaces of S_{Ref}, S_H and S_S groups for F specimens. The surface roughness was increased by hydration or submerged testing as well as the height of shear lips formed during the plastic deformation. S_a denotes the area surface roughness.

3.3. Applicability of results to other manufacturing setups

During 3D printing, the polymer is heated up above its melting temperature to be deposited onto the print bed [17], [27]. However, the temperature difference between the nozzle and environment results in a rapid cooling and causes the formation of an incomplete bond between filaments [17], [27]. Therefore, anisotropic mechanical properties are typically reported; an interface bond between 3D printed layers has much lower strength than any other direction [17], [27]. Applicability of obtained results to other manufacturing setups was investigated by measuring the mechanical properties of Z specimens (defined in Figure 2) to represent manufacturing induced-anisotropy by testing the failure of bonds between layers. These specimens (Figure 11b) were on average 12% weaker than the F ones (Figure 11a) due to incomplete fusion of extruded filaments during 3D printing as well as presence of stress-raisers between the two bonded filaments [23], [25], [26], [73]. The reference Z specimen (S^{Z}_{Ref}) failed abruptly (as shown in Figure 11b), since the fracture occurred at interface bond normal to the applied load [24], [47], [74]. Temperature had a greater effect on changing the slope of stress strain curves for Z specimens. Furthermore, submerged testing at body temperature (e.g. S^{Z}_{PHS}) illustrated some plasticity prior to failure compared with the sudden fracture for S^{Z}_{Ref}.

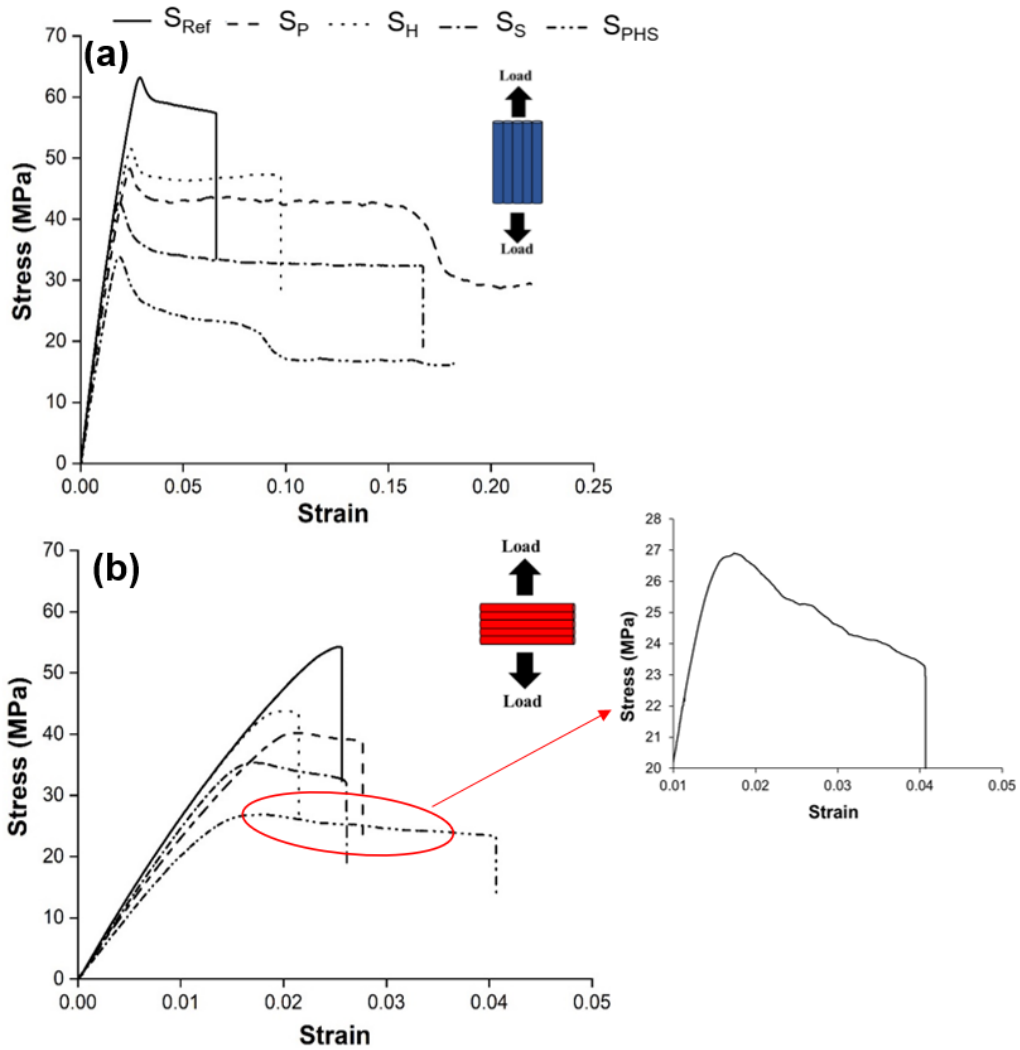

Figure 11 Representative stress-strain curves for F (a) and Z (b) specimens tested at different conditions. For both printing directions, S_{PHS} had the lowest strength value and the highest strain at break compared with S_{Ref}. The zoomed-in plastic region of stress strain curve for S^{Z}_{PHS} revealed fluctuations during the test.

The zoomed-in plastic deformation region of the stress-strain curve for S^Z_{PHS} (inset in Figure 11) shows some fluctuations in stress, which is discussed in relation to fractography shortly.

The main mechanical properties for Z specimens were calculated from the stress-strain curves; their statistical analysis is presented in Figure 12. Similar to the F specimens (Table 4), the least significant effect was observed for S^Z_H specimens. However, the change in the properties was still statistically significant for UTS ($p<0.01$), strain at maximum force ($p<0.05$) and strain at break ($p<0.01$), whilst the tensile modulus showed a negligible change ($p>0.05$) compared with the S^Z_{Ref}. In contrast to the F specimens, the hydrated Z specimens (S^Z_H) showed very little plasticity. This could be explained by the dependence of failure of the control specimens (S^Z_{Ref}) on the adhesion between extruded-filaments (i.e. interface bond) rather than the individual filaments, so brittle fracture was expected. The S^Z_P and S^Z_S specimens showed reduction in UTS, tensile modulus and strain at maximum force (all $p<0.001$ or $p<0.01$), possibly due to the higher chain mobility, but these conditions did not significantly affect strain at break ($p>0.05$). Although there was no significant difference between the strain at break values, the stress-strain curves (Figure 11b) were different. For the most plasticised specimens, yielding happened at lower strain, but demonstrated larger plastic strain post-yield behaviour. These two effects cancelled out each other, resulting in a relatively similar strain at break to S^Z_{Ref}.

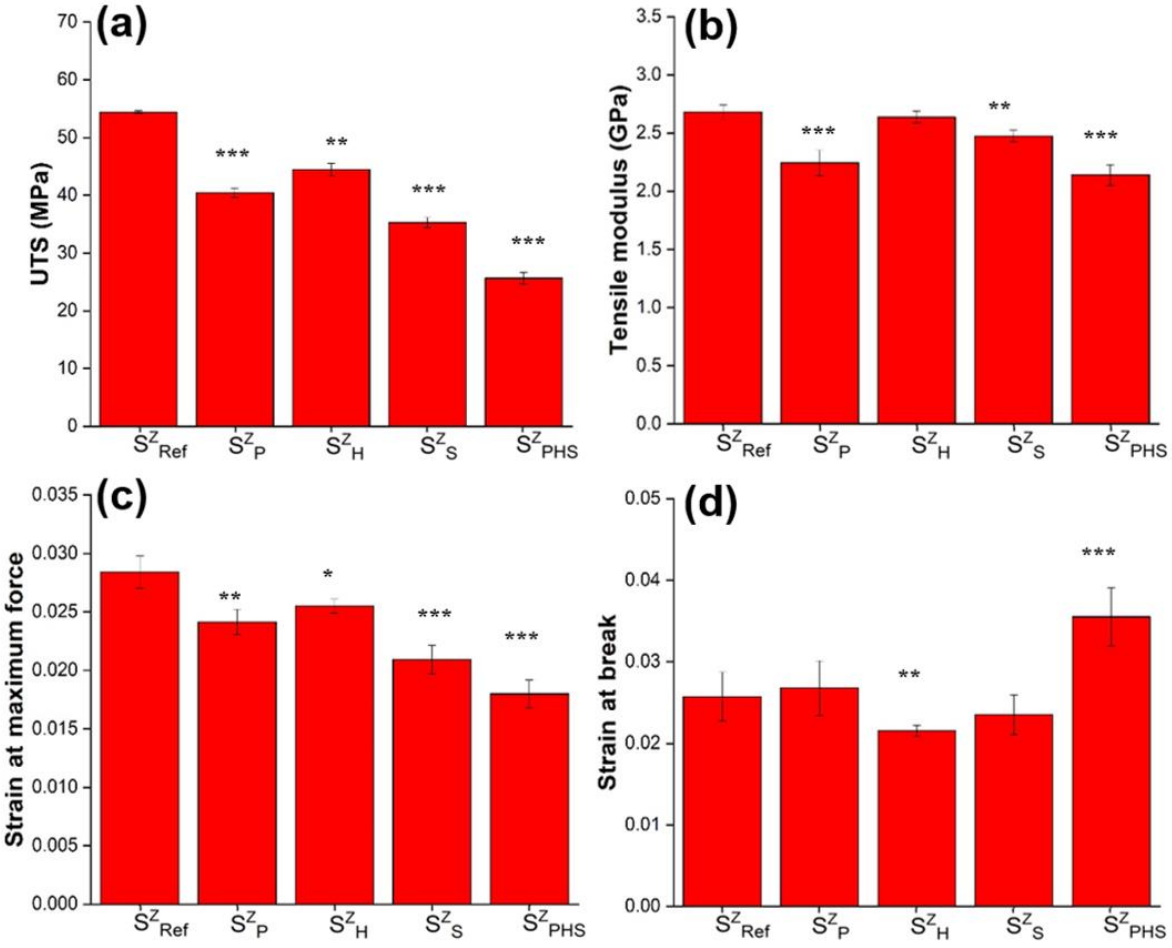

Figure 12 Mean UTS (a), tensile modulus (b), strain at maximum force (c) and strain at break for Z specimens tested at different testing conditions. Both temperature and moisture significantly affect the mechanical properties (* $p<0.05$, ** $p< 0.01$ and *** $p<0.001$ compared with S^Z_{Ref}).

The most significant ($p<0.001$) deterioration of properties was still observed for S^Z_{PHS} (Table 5). For this testing environment, even the level of strain at break was increased by approximately 30% compared to that of S^Z_{Ref}. The synergetic effect of high temperature and water absorption resulted in transition of brittle fracture to intermediate brittle-ductile one, which could also explain the fluctuations in stress recorded for the S^Z_{PHS} specimens.

Fractography analysis was also carried out for Z specimens. The optical micrographs showed a flat and smooth fracture surface, characteristic for brittle fracture [17], [24] as shown in Figure 13. The fracture surface of S^Z_{PHS}, however, was quite different compared with the others. The radial striations indicate the crack arrest, which could happen, when the stored strain energy was not adequate to drive the crack forwards; this is known as “pop in” crack propagation [75], [76]. These striations could further explain the fluctuations in stress recorded during tensile tests (Figure 11b). This process could be affected by plasticisation of polymer, which resulted in a significant increase in the strain at break compared to that of S^Z_{Ref}.

The characterisation of surface roughness and profile for the Z specimens are illustrated in Figure 13. The former was generally lower than that of the F specimens. The surface roughness of S^Z_{Ref} and S^Z_S were comparable, whilst, the one for S^Z_{PHS} was higher; indicating slight variations in the fracture. The surface profiles also confirmed the flat and smooth fracture surfaces except for S^Z_{PHS}. For this testing environment, apparent raised edges and micro-plasticity similar to those of the F specimens were observed, although of much smaller magnitude.

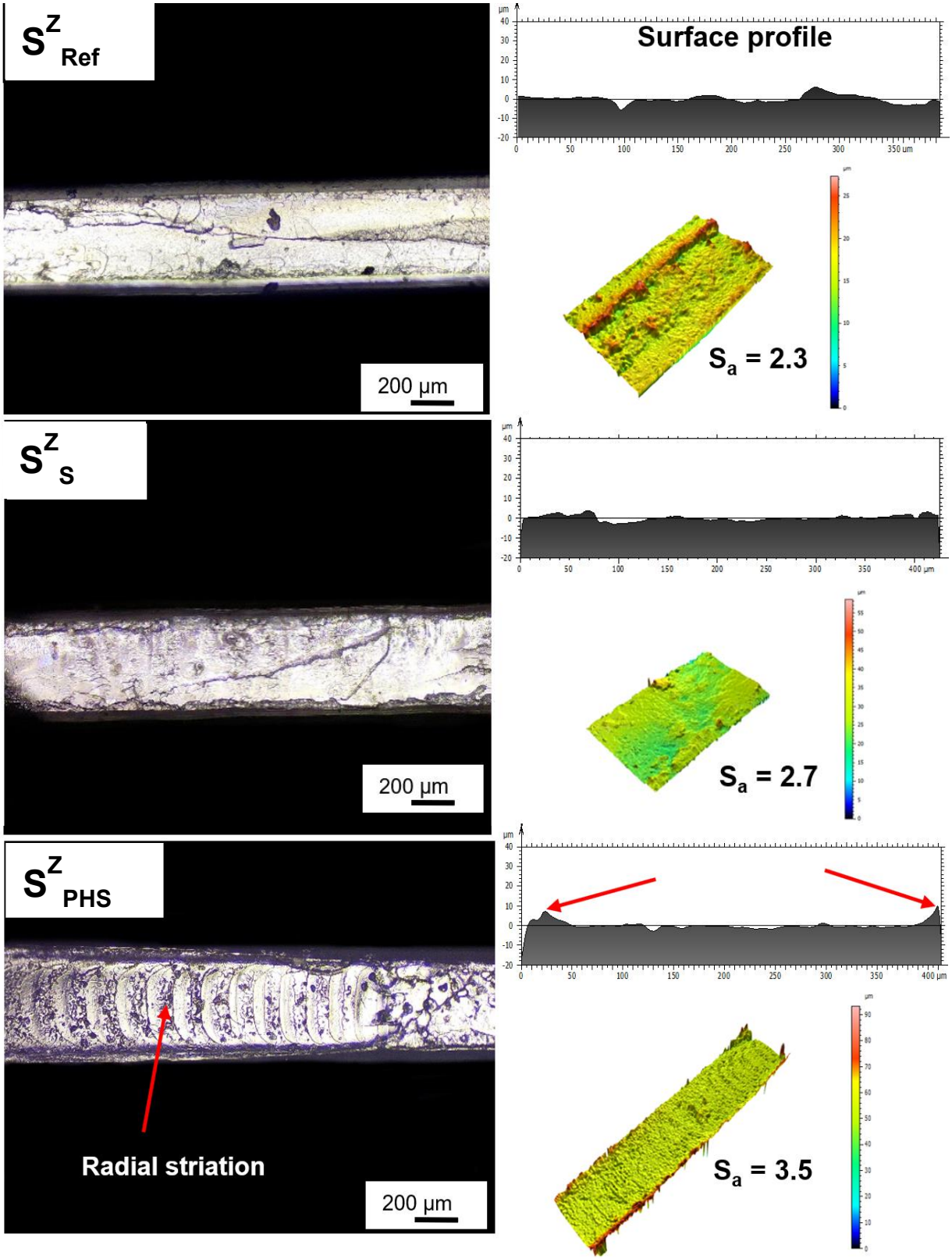

Figure 13 Optical microscopy images of fracture surfaces of Z specimens tested at different conditions. Since all specimens except S^Z_{PHS} showed very similar fracture characteristic, only the images for S^Z_{Ref}, S^Z_S and S^Z_{PHS} are shown here. S^Z_{PHS} demonstrated radial striations (shown by the arrows), which could have happened due to intermittent character of crack propagation. The surface profiles revealed the raised edges for S^Z_{PHS} similar to those of the F specimens indicating apparent shear lips. S_a denotes the area surface roughness.

From design perspective in order to account for any uncertainty, the part gets higher strength than it needs theoretically to have by employing a safety factor. This safety factor refers to the ratio of the allowed stress to actual in-service stress. In this study, a considerable reduction in the mechanical performance of 3D printed specimens in environment close to their applications was observed, which could not be identified in the commonly used testing environment for S_H specimens. To account for this, an adjustment to the safety factor was calculated (Table 6). It should be multiplied with the safety factor obtained based on the RT data (i.e. dry specimens). The calculation was done for S_{PHS} printed in F and Z directions which were the two extreme cases in additive manufactured parts (strongest and weakest orientations respectively).

For both extremes, the safety factor obtained under traditional testing condition should be effectively doubled in design of polymeric parts for the physiological environment (i.e. hydrated at high temperature). The summary of variation in different mechanical properties is given in Table 5. Apparently, hydration of specimens in water and testing them in air at RT (S_H), which was the most common method used in many studies, had the lowest effect compared with that of other factors on mechanical properties. Whereas, the combination of all three factors (S_{PHS}) resulted in the biggest effect on mechanical properties suggesting significant weakening of the polymer structure.

Table 5 Variation in mechanical properties for different testing conditions with respect to the printing orientation. NF = “no failure”.

Properties compared to S_{Ref}	Variation for different testing conditions (%)							
	PT (S_P)		Hydration (S_H)		Submerged (S_S)		All three (S_{PHS})	
	F	Z	F	Z	F	Z	F	Z
UTS	▼23%	▼26%	▼18%	▼18%	▼26%	▼34%	▼47%	▼50%
Tensile modulus	▼10%	▼15%	▼2%	▼2%	▼7%	▼7%	▼20%	▼20%
Strain @ max. force	▼15%	▼15%	▼10%	▼16%	▼26%	▼33%	▼37%	▼38%
Strain @ break	▲ NF	▲3%	▲31%	▼16%	▲37%	▼2%	▲ NF	▲29%

Table 6 Calculated adjustment to safety factors for both F and Z specimens.

Printing direction	Dry strength @ RT (MPa)	Wet strength @ PT (MPa)	Safety factor adjustment
F	62.6	33.1	1.89
Z	54.3	26.5	2.04

3.4. Applicability of results to bulk material properties

Applicability of the obtained results to bulk properties of PLA was investigated. In the literature, the UTS, tensile modulus and strain at break values range from 46.5 to 70.8 MPa, 1.90 to 3.21 GPa and 0.04 to 0.16 strain, respectively [77]–[85]. The strength and strain values of F specimens and bulk PLA obtained in previous studies [77]–[85] were plotted (Figure 14a). From the graph it is clear that the values obtained in the present study fitted well in this range (UTS was 63.4 MPa, tensile modulus was 2.31 GPa and strain at break was 0.071). For instance, in Figure 14b the stress-strain curve of F specimen in the present study is compared against that for the injection moulded PLA from another study [85] measured according to the ASTM D638 standard. Both curves showed very similar character, with differences of < 5 MPa in stress, which is considerably less than that reported in the literature. The novel 3D printed specimen used here demonstrated bulk materials properties. Therefore, the results can be applied to bulk properties; thus, considering the effect of environment of mechanical performance is critical for PLA components.

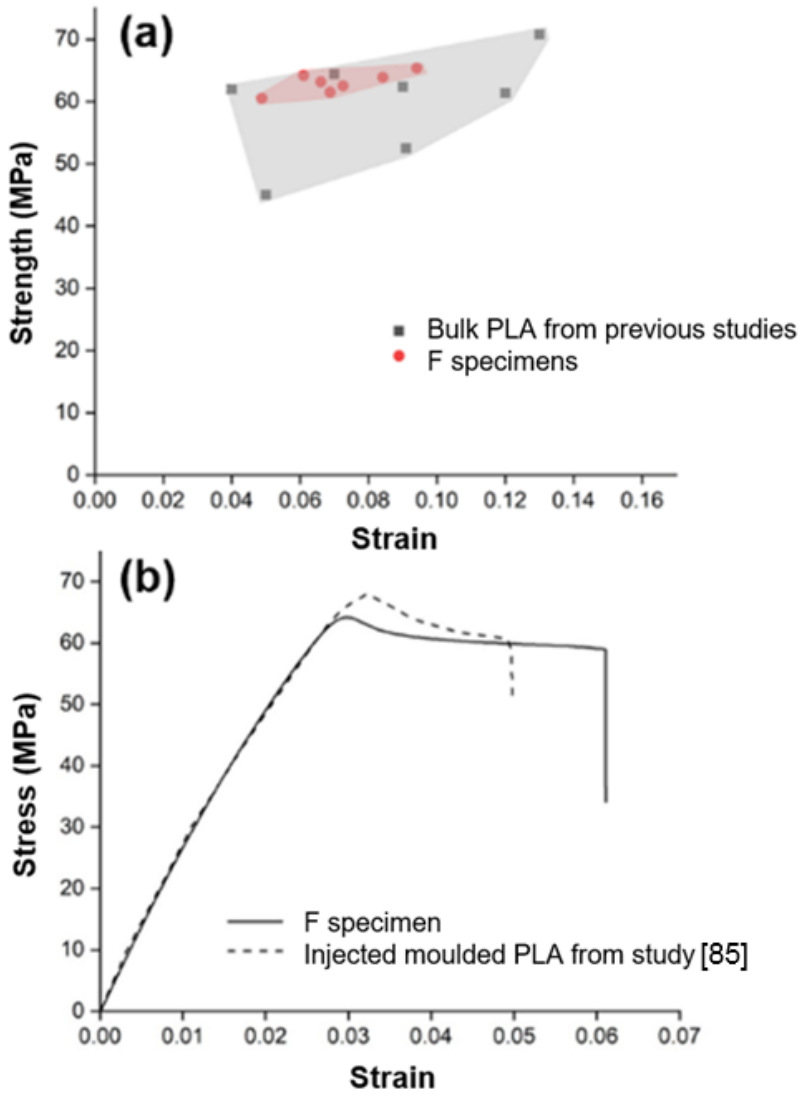

Figure 14 (a) Strength and strain values obtained in the present study for F specimens compared against the bulk PLA from previous studies [77]–[85]. (b) comparison between stress-strain curve of F specimens and injected moulded PLA from another study [85] indicating very similar character.

4. Conclusion

The effect of environment on mechanical properties of 3D printed PLA was investigated. The obtained results indicated the importance of submerged tensile testing to characterise the properties of polymers for biomedical application (i.e. physiological environment), where the material is exposed to higher temperature and surrounded by fluid. Submerged tests at 37°C approximately reduced the mechanical strength of polymer by 50%, its tensile modulus by 20% and allowed an extensive plastic deformation of polymer up to 40%. In contrast, measuring mechanical properties of the hydrated polymer in air at RT (which is often used to assess wet properties in the literature) only showed 18.1% reduction in the strength with no significant change in the modulus. The current methodology was also applied to other manufacturing designs to study the manufacturing-induced anisotropy. Similar trends were found for another orientation. The findings in this study clearly indicate that the commonly used methodology to measure the wet properties of polymer does not represent appropriately conditions in the body. Therefore, it is strongly recommended for future studies to employ submerged testing for characterisation of polymers for biomedical applications.

Supplementary results

The fracture progression of Z_{Ref} and F_{Ref} was monitored using a Thermo-sensorik CMT 384 infrared camera with 256 X 256 pixels with F/2.0 aperture (GmbH, Germany). The camera was calibrated prior to the test using two objects with known temperatures (one higher and one lower) to determine the upper and lower limits respectively. The contrast and brightness were optimised so that the fracture area would appear white (indication of higher temperature) and the other regions as black (indication of lower temperature). The stress-strain curves obtained from the tensile testing results indicated that PLA specimens showed anisotropic mechanical strength with respect to the printing orientation. Z specimens were on average 11% weaker than the F specimens (Figure S1). It was also apparent that the tensile modulus of the material did not change upon changing the printing orientation. However, Z specimens failed abruptly at a shorter strain of 2.51%, whilst the F specimen demonstrated a longer strain-at-break (6.54%). Monitoring the tensile testing using IR camera revealed different fracture progression. The IR image for Z specimens showed a sudden fracture with the release of some elastic strain energy in the upper region of the gauge (appeared as white lines) as indicated by the arrows (Figure S1a). On the other hand, the F specimens showed a slower and more localised crack propagation across the specimen (Figure S1b-d). The fractography analysis revealed a very flat and smooth fracture surface for the Z specimens with finer features at the top and bottom of the edges.

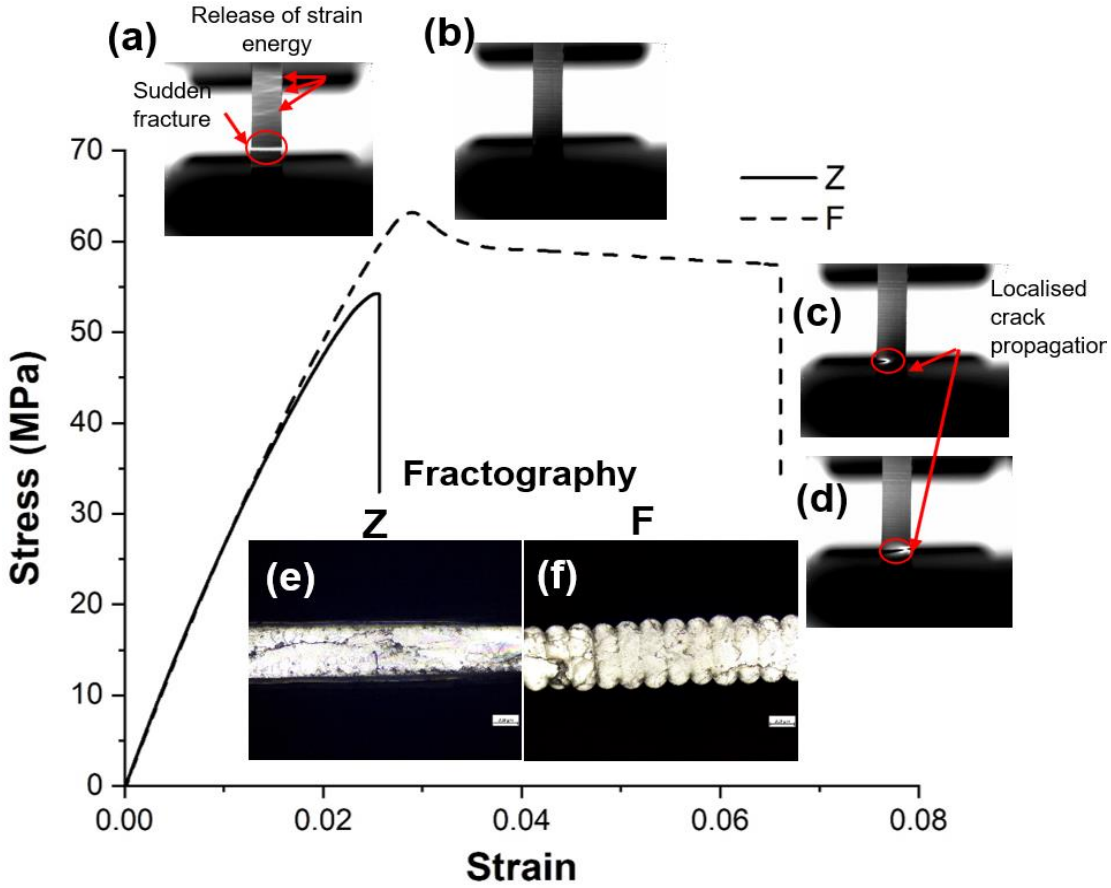

Figure S1 Representative stress-strain curve for Z (solid line) and F (dashed line) specimens. Z specimen showed the typical brittle fracture as it failed abruptly after 2.51% strain. F specimen underwent some plasticity prior to failure. a) IR image for Z indicated sudden fracture with release of elastic strain energy, whilst the images b-d indicated a localised crack propagation for F specimen. Optical images of the fracture surface for Z (e) and F (f) also supported IR images (the scale bar for fractography analysis images is 200 µm).

References:

[1] K. S. Anderson, S. H. Lim, and M. A. Hillmyer, “Toughening of polylactide by melt blending with linear low-density polyethylene,” *J. Appl. Polym. Sci.*, vol. 89, no. 14, pp. 3757–3768, 2003.

[2] K. Aou, S. L. Hsu, L. W. Kleiner, and F. W. Tang, “Roles of conformational and configurational defects on the physical aging of amorphous poly(lactic acid),” *J. Phys. Chem. B*, vol. 111, no. 42, pp. 12322–12327, 2007.

[3] D. Da Silva *et al.*, “Biocompatibility, biodegradation and excretion of polylactic acid (PLA) in medical implants and theranostic systems,” *Chem. Eng. J.*, vol. 340, pp. 9–14, 2018.

[4] S. Farah, D. G. Anderson, and R. Langer, “Physical and mechanical properties of PLA, and their functions in widespread applications — A comprehensive review,” *Adv. Drug Deliv. Rev.*, vol. 107, pp. 367–392, 2016.

[5] K. Madhavan Nampoothiri, N. R. Nair, and R. P. John, “An overview of the recent developments in polylactide (PLA) research.,” *Bioresour. Technol.*, vol. 101, no. 22, pp. 8493–501, 2010.

[6] H. Shui, Q. Shi, N. M. Pugno, Q. Chen, and Z. Li, “Effect of mechanical stimulation on the degradation of poly(lactic acid) scaffolds with different designed structures,” *J. Mech. Behav. Biomed. Mater.*, vol. 96, pp. 324–333, 2019.

[7] R. Jain, “The manufacturing techniques of various drug loaded biodegradable poly(lactide-co-glycolide) (PLGA) devices.,” *Biomaterials*, vol. 21, no. 23, pp. 2475–2490, 2000.

[8] S. Rathi, J. P. Kalish, E. B. Coughlin, and S. L. Hsu, “Utilization of oligo(lactic acid) for studies of chain conformation and chain packing in poly(lactic acid),” *Macromolecules*, vol. 44, no. 9, pp. 3410–3415, 2011.

[9] Z. Sheikh, S. Najeeb, Z. Khurshid, V. Verma, H. Rashid, and M. Glogauer, “Biodegradable materials for bone repair and tissue engineering applications,” *Materials (Basel).*, vol. 8, no. 9, pp. 5744–5794, 2015.

[10] K. Tappa and U. Jammalamadaka, “Novel biomaterials used in medical 3D printing techniques,” *J. Funct. Biomater.*, vol. 9, no. 1, pp. 1–17, 2018.

[11] K. Wang, C. C. Ho, C. Zhang, and B. Wang, “A Review on the 3D printing of functional structures for medical phantoms and regenerated tissue and organ applications,” *Engineering*, vol. 3, no. 5, pp. 653–662, 2017.

[12] K. Thrimurthulu, P. M. Pandey, and N. V. Reddy, “Optimum part deposition orientation in fused deposition modeling,” *Int. J. Mach. Tools Manuf.*, vol. 44, no. 6, pp. 585–594, 2004.

[13] A. A. Zadpoor, “Mechanics of additively manufactured biomaterials,” *J. Mech. Behav. Biomed. Mater.*, vol. 70, pp. 1–6, 2017.

[14] L. Safai, J. S. Cuellar, G. Smit, and A. A. Zadpoor, “A review of the fatigue behavior of 3D printed polymers,” *Addit. Manuf.*, vol. 28, pp. 87–97, 2019.

[15] S. C. Ligon, R. Liska, J. Stampfl, M. Gurr, and R. Mülhaupt, “Polymers for 3D printing and customized additive manufacturing,” *Chem. Rev.*, vol. 117, no. 15, pp. 10212–10290, 2017.

[16] J. Garcia, Z. Yang, R. Mongrain, R. L. Leask, and K. Lachapelle, “3D printing materials and their use in medical education: a review of current technology and trends for the future,” *BMJ Simul. Technol. Enhanc. Learn.*, vol. 4, no. 1, pp. 27–40, 2018.

[17] A. Gleadall, W. Poon, J. Allum, A. Ekinci, X. Han, and V. V. Silberschmidt, “Interfacial fracture of 3D-printed bioresorbable polymers,” *Procedia Struct. Integr.*, vol. 13, pp. 625–630, 2018.

[18] P. Wang, B. Zou, H. Xiao, S. Ding, and C. Huang, “Effects of printing parameters of fused deposition modeling on mechanical properties, surface quality, and microstructure of PEEK,” *J. Mater. Process. Technol.*, vol. 271, pp. 62–74, 2019.

[19] L. Ruiz-cantu, A. Gleadall, C. Faris, J. Segal, K. Shakesheff, and J. Yang, “Characterisation of the surface structure of 3D printed scaffolds for cell in filtration and surgical suturing,” *Biofabrication*, vol. 8, no. 1, pp. 1–12, 2016.

[20] X. Wang, M. Jiang, Z. Zhou, J. Gou, and D. Hui, “3D printing of polymer matrix composites: A review and prospective,” *Compos. Part B Eng.*, vol. 110, pp. 442–458, 2017.

[21] J. J. Laureto and J. M. Pearce, “Anisotropic mechanical property variance between ASTM D638-14 type i and type iv fused filament fabricated specimens,” *Polym. Test.*, vol. 68, pp. 294–301, 2018.

[22] Y. Song, Y. Li, W. Song, K. Yee, K. Y. Lee, and V. L. Tagarielli, “Measurements of the mechanical response of unidirectional 3D-printed PLA,” *Mater. Des.*, vol. 123, pp. 154–164, 2017.

[23] S. H. Ahn, C. Baek, S. Lee, and I. S. Ahn, “Anisotropic tensile failure model of rapid prototyping parts - Fused deposition modeling (FDM),” *Int. J. Mod. Phys. B*, vol. 17, no. 08n09, pp. 1510–1516, 2003.

[24] J. M. Chacón, M. A. Caminero, E. García-Plaza, and P. J. Núñez, “Additive manufacturing of PLA structures using fused deposition modelling: Effect of process parameters on mechanical properties and their optimal selection,” *Mater. Des.*, vol. 124, pp. 143–157, 2017.

[25] H. Li, T. Wang, J. Sun, and Z. Yu, “The effect of process parameters in fused deposition modelling on bonding degree and mechanical properties,” *Rapid Prototyp. J.*, vol. 24, no. 1, pp. 80–92, 2018.

[26] J. Torres, M. Cole, A. Owji, Z. DeMastry, and A. P. Gordon, “An approach for mechanical property optimization of fused deposition modeling with polylactic acid via design of experiments,” *Rapid Prototyp. J.*, vol. 22, no. 2, pp. 387–404, 2016.

[27] T. J. Coogan and D. O. Kazmer, “Bond and part strength in fused deposition modeling,” *Rapid Prototyp. J.*, vol. 23, no. 2, pp. 414–422, 2017.

[28] L. Wu, J. Zhang, D. Jing, and J. Ding, “‘Wet-state’ mechanical properties of three-dimensional polyester porous scaffolds,” *J. Biomed. Mater. Res. - Part A*, vol. 76, no. 2, pp. 264–271, 2006.

[29] M. A. Elsawy, K. H. Kim, J. W. Park, and A. Deep, “Hydrolytic degradation of polylactic acid (PLA) and its composites,” *Renew. Sustain. Energy Rev.*, vol. 79, pp. 1346–1352, 2017.

[30] M. A. Paul, C. Delcourt, M. Alexandre, P. Degée, F. Monteverde, and P. Dubois, “Polylactide/montmorillonite nanocomposites: Study of the hydrolytic degradation,” *Polym. Degrad. Stab.*, vol. 87, no. 3, pp. 535–542, 2005.

[31] G. Schliecker, C. Schmidt, S. Fuchs, and T. Kissel, “Characterization of a homologous series of D,L-lactic acid oligomers; a mechanistic study on the degradation kinetics in vitro,” *Biomaterials*, vol. 24, no. 21, pp. 3835–3844, 2003.

[32] O. Vyavahare, D. Ng, and S. L. Hsu, “Analysis of structural rearrangements of poly(lactic acid) in the presence of water,” *J. Phys. Chem. B*, vol. 118, no. 15, pp. 4185–4193, 2014.

[33] S. St. Lawrence, J. L. Willett, and C. J. Carriere, “Effect of moisture on the tensile properties of poly(hydroxy ester ether),” *Polymer (Guildf).*, vol. 42, no. 13, pp. 5643–5650, 2001.

[34] J. C. Middleton and A. J. Tipton, “Synthetic biodegradable polymers as orthopedic devices,” *Biomaterials*, vol. 21, no. 23, pp. 2335–2346, 2000.

[35] C. Zhou *et al.*, “Temperature dependence of poly(lactic acid) mechanical properties,” *RSC Adv.*, vol. 6, no. 114, pp. 113762–113772, 2016.

[36] A. Le Duigou, P. Davies, and C. Baley, “Seawater ageing of flax/poly(lactic acid) biocomposites,” *Polym. Degrad. Stab.*, vol. 94, no. 7, pp. 1151–1162, 2009.

[37] V. K. Holm, S. Ndoni, and J. Risbo, “The stability of poly(lactic acid) packaging films as influenced by humidity and temperature,” *J. Food Sci.*, vol. 71, no. 2, pp. 40–44, 2006.

[38] G. H. Yew, A. M. Mohd Yusof, Z. A. Mohd Ishak, and U. S. Ishiaku, “Water absorption and enzymatic degradation of poly(lactic acid)/rice starch composites,” *Polym. Degrad. Stab.*, vol. 90, no. 3, pp. 488–500, 2005.

[39] Á. Sonseca, O. Menes, and E. Giménez, “A comparative study of the mechanical, shape-memory, and degradation properties of poly(lactic acid) nanofiber and cellulose nanocrystal reinforced poly(mannitol sebacate) nanocomposites,” *RSC Adv.*, vol. 7, no. 35, pp. 21869–21882, 2017.

[40] A. Abdal-Hay, M. G. Hwang, and J. K. Lim, “In vitro bioactivity of titanium implants coated with bicomponent hybrid biodegradable polymers,” *J. Sol-Gel Sci. Technol.*, vol. 64, no. 3, pp. 756–764, 2012.

[41] K. Nagahama, K. Shimizu, S. Ichimura, A. Takahashi, T. Ouchi, and Y. Ohya, “Biodegradable stereocomplex materials of polylactide-grafted dextran exhibiting soft and tough properties in dry and wet states,” *J. Polym. Sci. Part A Polym. Chem.*, vol. 50, no. 13, pp. 2669–2676, 2012.

[42] A. B. Kutikov, A. Gurijala, and J. Song, “Rapid Prototyping Amphiphilic Polymer/Hydroxyapatite Composite Scaffolds with Hydration-Induced Self-Fixation Behavior,” *Tissue Eng. Part C Methods*, vol. 21, no. 3, pp. 229–241, 2014.

[43] Y. Wan, Q. Wu, S. Wang, S. Zhang, and Z. Hu, “Mechanical properties of porous polylactide/ chitosan blend membranes,” *Macromol. Mater. Eng.*, vol. 292, no. 5, pp. 598–607, 2007.

[44] X. F. Zhang, H. O’Shea, S. Kehoe, and D. Boyd, “Time-dependent evaluation of mechanical properties and in vitro cytocompatibility of experimental composite-based nerve guidance conduits,” *J. Mech. Behav. Biomed. Mater.*, vol. 4, no. 7, pp. 1266–1274, 2011.

[45] N. Zhang, Y. Wang, W. Xu, Y. Hu, and J. Ding, “Poly(lactide-co-glycolide)/hydroxyapatite porous scaffold with microchannels for bone regeneration,” *Polymers (Basel).*, vol. 8, no. 6, 2016.

[46] X. Wang *et al.*, “Fabrication and characterization of poly(l-lactide-co-glycolide) knitted mesh-reinforced collagen-chitosan hybrid scaffolds for dermal tissue engineering,” *J. Mech. Behav. Biomed. Mater.*, vol. 8, pp. 204–215, 2012.

[47] E. Kim, Y. J. Shin, and S. H. Ahn, “The effects of moisture and temperature on the mechanical properties of additive manufacturing components: Fused deposition modeling,” *Rapid Prototyp. J.*, vol. 22, no. 6, pp. 887–894, 2016.

[48] R. M. Felfel, I. Ahmed, A. J. Parsons, G. S. Walker, and C. D. Rudd, “In vitro degradation, flexural, compressive and shear properties of fully bioresorbable composite rods,” *J. Mech. Behav. Biomed. Mater.*, vol. 4, no. 7, pp. 1462–1472, 2011.

[49] W. Xu, R. Shen, Y. Yan, and J. Gao, “Preparation and characterization of electrospun alginate/PLA nanofibers as tissue engineering material by emulsion eletrospinning,” *J. Mech. Behav. Biomed. Mater.*, vol. 65, pp. 428–438, 2017.

[50] D. Bellini *et al.*, “PLA-grafting of collagen chains leading to a biomaterial with mechanical performances useful in tendon regeneration,” *J. Mech. Behav. Biomed. Mater.*, vol. 64, pp. 151–160, 2016.

[51] T. Andric, B. L. Taylor, A. R. Whittington, and J. W. Freeman, “Fabrication and characterization of three-dimensional electrospun scaffolds for bone tissue engineering,” *Regen. Eng. Transl. Med.*, vol. 1, no. 1–4, pp. 32–41, 2015.

[52] L. Hartmann *et al.*, “Toward the development of an artificial cornea: Improved stability of interpenetrating polymer networks,” *J. Biomed. Mater. Res. - Part B Appl. Biomater.*, vol. 98 B, no. 1, pp. 8–17, 2011.

[53] B. N. Singh, N. N. Panda, R. Mund, and K. Pramanik, “Carboxymethyl cellulose enables silk fibroin nanofibrous scaffold with enhanced biomimetic potential for bone tissue engineering application,” *Carbohydr. Polym.*, vol. 151, pp. 335–347, 2016.

[54] V. E. Bosio, J. Brown, M. J. Rodriguez, and D. L. Kaplan, “Biodegradable porous silk microtubes for tissue vascularization,” *J. Mater. Chem. B*, vol. 5, no. 6, pp. 1227–1235, 2017.

[55] P. J. Wang *et al.*, “Effect of working environment and procedural strategies on mechanical performance of bioresorbable vascular scaffolds,” *Acta Biomater.*, vol. 82, pp. 34–43, 2018.

[56] J. F. Fuzek, “Absorption and desorption of water by some common fibers,” *Ind. Eng. Chem. Prod. Res. Dev.*, vol. 24, no. 1, pp. 140–144, 1985.

[57] H. E. Bair, G. E. Johnson, and R. Merriweather, “Water sorption of polycarbonate and its effect on the polymer’s dielectric behavior,” *J. Appl. Phys.*, vol. 49, no. 10, pp. 4976–4984, 1978.

[58] W. N. Ayre, S. P. Denyer, and S. L. Evans, “Ageing and moisture uptake in polymethyl methacrylate (PMMA) bone cements,” *J. Mech. Behav. Biomed. Mater.*, vol. 32, pp. 76–88, 2014.

[59] M. Grasso, L. Azzouz, P. Ruiz-Hincapie, M. Zarrelli, and G. Ren, “Effect of temperature on the mechanical properties of 3D-printed PLA tensile specimens,” *Rapid Prototyp. J.*, vol. 24, no. 8, pp. 1337–1346, 2018.

[60] M. J. Kendall and C. R. Siviour, “Rate dependence of poly(vinyl chloride), the effects of plasticizer and time-temperature superposition,” *Proc. R. Soc. A Math. Phys. Eng. Sci.*, vol. 470, no. 2167, p. 20140012, 2014.

[61] H. Sehaqui, T. Zimmermann, and P. Tingaut, “Hydrophobic cellulose nanopaper

through a mild esterification procedure," *Cellulose*, vol. 21, no. 1, pp. 367–382, 2014.

[62] A. Onur, A. Ng, G. Garnier, and W. Batchelor, "The use of cellulose nanofibres to reduce the wet strength polymer quantity for development of cleaner filters," *J. Clean. Prod.*, vol. 215, pp. 226–231, 2019.

[63] M. Nikzad, S. H. Masood, and I. Sbarski, "Thermo-mechanical properties of a highly filled polymeric composites for Fused Deposition Modeling," *Mater. Des.*, vol. 32, no. 6, pp. 3448–3456, 2011.

[64] J. L. Yang, Z. Zhang, A. K. Schlarb, and K. Friedrich, "On the characterization of tensile creep resistance of polyamide 66 nanocomposites. Part I. Experimental results and general discussions," *Polymer (Guildf).*, vol. 47, no. 8, pp. 2791–2801, 2006.

[65] P. Khalili, X. LIU, Z. ZHAO, and B. Blinzler, "Fully biodegradable composites: thermal, flammability, moisture absorption and mechanical properties of natural fibre-reinforced composites with nano-hydroxyapatite," *Materials (Basel).*, vol. 12, no. 7, p. 1145, 2019.

[66] Y. B. Tee, R. A. Talib, K. Abdan, N. L. Chin, R. K. Basha, and K. F. Md Yunos, "Effect of aminosilane concentrations on the properties of poly (Lactic Acid)/Kenaf-derived cellulose composites," *Polym. Polym. Compos.*, vol. 25, no. 1, pp. 63–76, 2017.

[67] M. Deroiné *et al.*, "Accelerated ageing of polylactide in aqueous environments: Comparative study between distilled water and seawater," *Polym. Degrad. Stab.*, vol. 108, no. July 2018, pp. 319–329, 2014.

[68] A. Lanzotti, M. Grasso, G. Staiano, and M. Martorelli, "The impact of process parameters on mechanical properties of parts fabricated in PLA with an open-source 3-D printer," *Rapid Prototyp. J.*, vol. 21, no. 5, pp. 604–617, 2015.

[69] S. Saeidlou, M. A. Huneault, H. Li, and C. B. Park, "Poly(lactic acid) crystallization," *Prog. Polym. Sci.*, vol. 37, no. 12, pp. 1657–1677, 2012.

[70] J. C. Halpin and J. L. Kardos, "Moduli of crystalline polymers employing composite theory," *J. Appl. Phys.*, vol. 43, no. 5, pp. 2235–2241, 1972.

[71] A. Herrera-Gómez, G. Velázquez-Cruz, and M. O. Martín-Polo, "Analysis of the water bound to a polymer matrix by infrared spectroscopy," *J. Appl. Phys.*, vol. 89, no. 10, pp. 5431–5437, 2001.

[72] D. Arencón and J. I. Velasco, "Fracture toughness of polypropylene-based particulate composites," *Materials (Basel).*, vol. 2, no. 4, pp. 2046–2094, 2009.

[73] J. Allum, A. Gleadall, and V. Silberschmidt, "Fracture of 3D-printed polymers: crucial role of filament-scale geometric features (submitted for publication)."

[74] B. Rankouhi, S. Javadpour, F. Delfanian, and T. Letcher, "Failure analysis and mechanical characterization of 3D printed ABS with respect to layer thickness and orientation," *J. Fail. Anal. Prev.*, vol. 16, no. 3, pp. 467–481, 2016.

[75] R. J. Parrington, "Fractography of metals and plastics," *Pract. Fail. Anal.*, vol. 2, no. 5, pp. 16–19, 2002.

[76] W. T. Becker and S. Lampman, *ASM Handbook Volume 11: Failure Analysis and Prevention*, 10th ed. ASM International, 2002.

[77] H. Pan *et al.*, "The effect of MDI on the structure and mechanical properties of poly(lactic acid) and poly(butylene adipate-co-butylene terephthalate) blends," *RSC Adv.*, vol. 8, no. 9, pp. 4610–4623, 2018.

[78] Y. Bin, B. Yang, and H. Wang, “The effect of a small amount of modified microfibrillated cellulose and ethylene–glycidyl methacrylate copolymer on the crystallization behaviors and mechanical properties of polylactic acid,” *Polym. Bull.*, vol. 75, no. 8, pp. 3377–3394, 2018.

[79] X. Meng, N. A. Nguyen, H. Tekinalp, E. Lara-Curzio, and S. Ozcan, “Supertough PLA-silane nanohybrids by in situ condensation and grafting,” *ACS Sustain. Chem. Eng.*, vol. 6, no. 1, pp. 1289–1298, 2018.

[80] C. Zhang, Y. Huang, C. Luo, L. Jiang, and Y. Dan, “Enhanced ductility of polylactide materials: Reactive blending with pre-hot sheared natural rubber,” *J. Polym. Res.*, vol. 20, no. 4, pp. 121–130, 2013.

[81] T. Y. Qiu, M. Song, and L. G. Zhao, “Testing, characterization and modelling of mechanical behaviour of poly (lactic-acid) and poly (butylene succinate) blends,” *Mech. Adv. Mater. Mod. Process.*, vol. 2, no. 1, pp. 1–11, 2016.

[82] N. Graupner, “Application of lignin as natural adhesion promoter in cotton fibre-reinforced poly(lactic acid) (PLA) composites,” *J. Mater. Sci.*, vol. 43, no. 15, pp. 5222–5229, 2008.

[83] H. Zhang *et al.*, “Preparation, characterization and properties of PLA/TiO2 nanocomposites based on a novel vane extruder,” *RSC Adv.*, vol. 5, no. 6, pp. 4639–4647, 2015.

[84] I. Restrepo, N. Benito, C. Medinam, R. V. Mangalaraja, P. Flores, and S. Rodriguez-Llamazares, “Development and characterization of polyvinyl alcohol stabilized polylactic acid/ZnO nanocomposites,” *Mater. Res. Express*, vol. 4, no. 10, pp. 1–8, 2017.

[85] W. Song, H. Liu, F. Chen, and J. Zhang, “Effects of ionomer characteristics on reactions and properties of poly(lactic acid) ternary blends prepared by reactive blending,” *Polymer (Guildf).*, vol. 53, no. 12, pp. 2476–2484, 2012.